Mémoire

Auteur : Meziane, Elias
Promoteur(s) : Cudell, Jean-Rene
Faculté : Faculté des Sciences
Diplôme : Master en sciences spatiales, à finalité approfondie
Année académique : 2021-2022
URI/URL : http://hdl.handle.net/2268.2/16123

Scalar clouds around spinning black holes

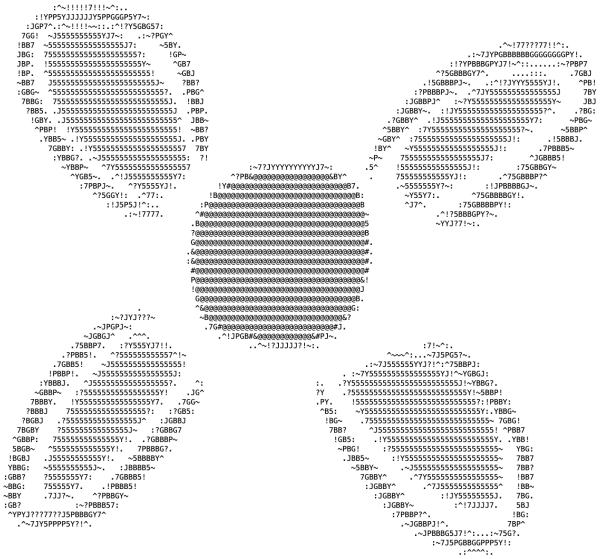

Elias Meziane

A Master thesis presented in partial fulfilment of the requirements for the Degree of *Master in Space Sciences*

University of Liège

Academic year 2021-2022

Loaded training module.
-Népal
445e Nuit, 2017

Acknowledgement

I would like to thank my promoter Prof. Jean-René Cudell for accompanying me throughout this journey and for his good mood, more contagious than a particular virus. I would also like to thank my reading committee composed of Prof. Maxime Fays, Prof. Peter Schlagheck, and Prof. Denis Grodent, for dedicating a part of your time to read my dissertation.
My thoughts go to my family, without who I would not be writing this sentence... More seriously, I can only thank my family for Everything, although it would be impossible to reciprocate, even if I had the seven lives of a cat. Thanks to my friends, and to my high school physics teacher Jean-François Claeskens for giving me his curiosity and passion for physics.

Contents

Introduction

The dark matter paradigm

Our universe is home to countless galaxies organized in different structures according to the number of galaxies they contain. These galaxies are held together by mutual gravitational attraction to form the smallest aggregate of galaxies called groups. These groups contain no less than fifty galaxies and extend over 5 million light-years. They then associate to form clusters containing not less than a few thousand galaxies over 10 million light-years. If we continue to step back, we notice that these groups and clusters, along with a few isolated galaxies, are grouped on a larger scale into even larger structures, the superclusters. For example, our Milky Way belongs to the Local group, which in turn is part of the Virgo cluster, which is part of the Virgo supercluster that is part of the Laniakea supercluster. At the cosmological scale, superclusters combine in a network of galactic filaments and form the cosmic web. They may span between several hundred million light-years to 10 billion light-years and are the largest structures known to date. In this section, we will see that matter (or energy) is missing at many scales. Let us start with a familiar habitat, the galaxies.

Galaxy rotation curves

Edwin Hubble classified galaxies according to their morphology in 1926, based on their appearance on a photographic plate. This is the well-known Hubble sequence that splits galaxies into irregular, elliptical, spiral, and barred spiral morphologies [1]. In 1978, the American astronomer Vera Rubin, notably called the "mother of dark matter", measured the rotation curves of high-luminosity spiral galaxies via the Doppler shift of H-α emission lines [2]. Based on the visible mass content of these galaxies, the tendency would be a decreasing radial velocity with the distance from the galactic center. Surprisingly, these galaxies are spinning too fast. Indeed, Vera Rubin and her team highlighted that the velocity profile is flat in the external arms [2]. It is thus intuitive to postulate the existence of invisible mass so that the radial velocity profile is consistent with the observations. This missing mass would take the form of a halo around these galaxies. A hypothesis once considered was a galactic halo made of bodies that emit little or no radiation and drift through interstellar space unassociated with any planetary system. These are MACHOs (Massive Astrophysical Compact Halo Objects) and include black holes, brown dwarfs, and rogue planets. They can be detected via gravitational microlensing. When they pass in front of a star, the MACHO's gravity bends the background light, causing the star to appear brighter. Based on this technique, no more than 20% of matter in the galactic halo is expected from MACHOs [3]. Moreover, the primordial nucleosynthesis predicted

the abundances of light elements, depending on the matter density. It turns out that the density for which all the predicted abundances agree with the observations is higher than the observed one [4]. Therefore, there should exist invisible matter in the Universe. We must look beyond the standard model and think of dark matter.

Clusters and collisions

Dark matter also appears to be present at larger scales in galaxy clusters. In 1933, the Swiss astronomer Fritz Zwicky measured radial velocities of galaxies in the Coma cluster via the Doppler effect [5]. He obtained a velocity dispersion around 1000 km/s. With such velocities, in order for the galaxies to remain gravitationally bound to the cluster, one needs a total mass greater than the visible mass. Fritz Zwicky highlighted this gravitational anomaly. Moreover, galactic dark matter halos are not massive enough to fill the gap. Consequently, there must be additional matter, distributed in between the galaxies of the Coma cluster.

Figure 1: From [6]. Dark matter map of the galaxy cluster Abell 1689 (in purple) superimposed over background galaxies obtained via gravitational lensing.

Another extragalactic manifestation of dark matter can be found in the Bullet cluster, which consists of two colliding clusters of galaxies (cf. Figure 2). These are rare and extreme events in which the bulk of the baryonic matter becomes displaced from the dark matter halos of the colliding subclusters. The major mass components of the Bullet cluster are stars, gas, and the putative dark matter. Each component behaves differently during the collision, allowing them to be studied separately. The stars of the galaxies, seen in visible light, are not greatly affected by the collision, and most passed right through. The hot gas within each cluster, observable in X-rays, represents most of the baryonic matter. The gas in each cluster interacts via electromagnetism, causing the gases of both clusters to slow down much more than the stars. Finally, the dark matter was detected indirectly via the weak gravitational lensing of background objects. In theories without dark matter, the lensing is expected to follow the baryonic matter, i.e. principally the X-ray gas. However, the lensing is strongest in two separated regions near the visible galaxies. It provides support to the idea that most of the gravitation in the cluster pair is in the form of two regions of dark matter, which bypassed the gas regions during

the collision. It accords with predictions of dark matter as only weakly gravitationally interacting.

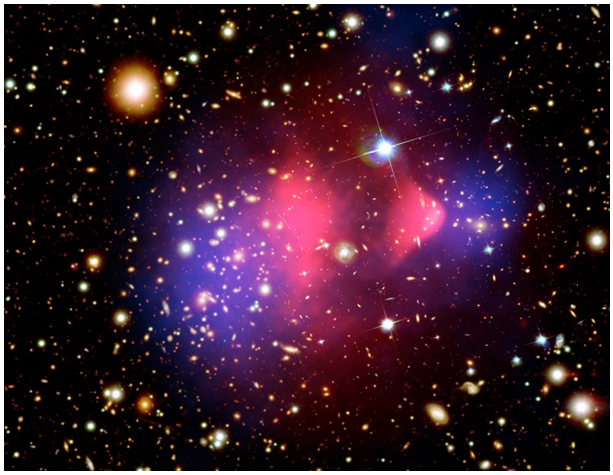

Figure 2: From [7]. X-ray image of the Bullet Cluster (in pink) superimposed over a visible light image of galaxies, with matter distribution, including baryonic and dark matter, inferred from gravitational lensing (in blue).

A challenge to the dark matter paradigm appears with Abell 520, a merging cluster system at 2.4 billion light-years away (cf. Figure 3). It has been popularly nicknamed the "train wreck" cluster, because of its chaotic substructure. The latter is rather surprising since it should contain a central region principally made of dark matter, namely a "dark core", where there is no significant concentration of bright galaxies [8]. Abell 520 thus seems in contradiction with the collisionless dark matter scenario. Our current understanding of dark matter could not explain this dark core at the center of Abell 520. Maybe dark matter does not exist after all? Is it a missing piece of the standard model, or clues that our theory of gravity is obsolete at large scales? We could make this bet, but turning back require a consistent theory able to explain the radial velocity profile of stars within galaxies, the dynamics of the Coma cluster, or the very structure of the Bullet cluster. A possibility is a type of dark matter with larger interactions and pressure, that is more concentrated in Abell 520 than in the Bullet Cluster. Or simply the puzzling "dark core" may not be so dark. A recent analysis suggests that the dark matter to baryonic matter ratio is around 2, in agreement with typical values for galaxies with dark matter, while the original study suggests a 6-to-1 ratio [9]. A subsequent analysis in 2017 proposes that dark matter may not be localized at the center of the merging cluster and is more diffuse [10]. In conclusion, the merging cluster system Abell 520 may not cause a significant problem to the collisionless dark matter scenario.

Cosmic web and beyond

Contemporary cosmological models are based on the Copernican principle. There are no privileged observers in the Universe: it looks the same from everywhere on a very large scale. Deconstructing our central role in the cosmos has opened the way to a more general principle, the cosmological principle. The postulate that the Universe is homogeneous and isotropic was then used as a pillar to develop a theory describing the dynamics of our Universe in its entirety. A scientific argument supporting this postulate is of course the

Figure 3: From [8]. X-ray image of Abell 520 and its hot gas (in green) superimposed over a visible light image of galaxies within the cluster, baryonic matter (in orange), and dark matter inferred from gravitational lensing (in blue). Contrary to the Bullet Cluster, we observe that dark matter is located at the center and not in the external regions where galaxies are more concentrated.

cosmic microwave background and its impressive homogeneity in all directions [11]. It was not until the advent of general relativity that the cosmological principle came to the fore. In the early 1920s, the Soviet mathematician Alexander Friedmann derived a dynamical model based on it [12][13]. However, his work remained relatively unnoticed by its contemporaries and Friedmann died in 1925. Later in 1927, a Belgian priest, astronomer and physicist Georges Lemaître arrived at results similar to those of Friedmann, while Albert Einstein did not agree with the physics of the model [14]. Thanks to the context of the discovery of the expansion of the Universe by Edwin Hubble during these years, his article aroused the interest of the scientific community. His work was translated into English and published in Monthly Notices of the Royal Astronomical Society in 1931 [15]. During the 1930s, the American mathematician Howard Robertson and his British colleague Arthur G.Walker rigorously proved in a series of articles the unicity of the homogeneous and isotropic metric obtained by Lemaître and Friedmann [16][17][18][19]. The general metric called the Friedmann-Lemaître-Robertson-Walker (FLRW) metric, in chronological order of the contributions, along with the Friedmann-Lemaître model, presently constitutes the most accurate description of the dynamics of our Universe.

A homogeneous and isotropic Universe puts constraints on its energy-matter content. A popular treatment is to consider our Universe filled with a perfect fluid. Components of this energy-matter ocean are baryonic, dark matter and radiation, i.e. photons and relativistic particles. There is another candidate that is sometimes considered, which is the vacuum itself. Thanks to weak gravitational lensing surveys over thousands of galaxies and simulations of the standard cosmological model, dark matter should be organized into filaments, in agreement with the cosmic web picture [20] [21] (cf. Figure 4). Beyond matter and radiation, an antagonist component to gravity is required to explain the accelerated expansion of the Universe, namely dark energy. It should have negative pressure and fill most of the Universe. Note that dark energy is at the heart of a strong scientific disagreement between observations and theory concerning vacuum energy. Whereas some scientists suggest a new treatment to gravity at cosmological scales or seek a particular scalar field, solving the dark matter problems may come with dark energy. These unknowns might be the two sides of the same coin.

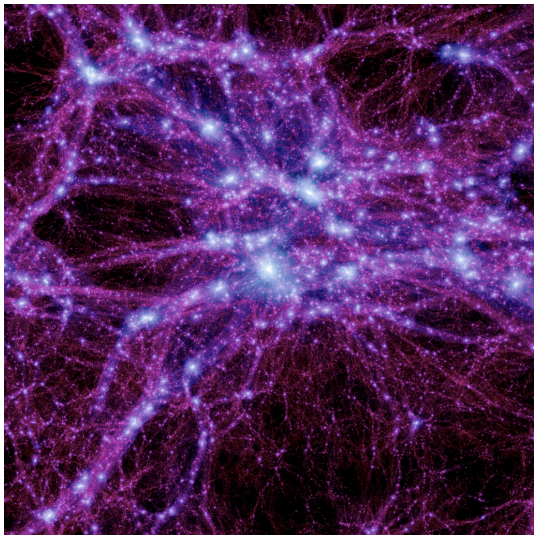

Figure 4: From [21]. Simulation of dark matter distribution based on the FLRW spacetime. Bright spots are visible matter (galaxies) while purple filaments correspond to dark matter. Dark matter filaments gravitationally attract baryonic matter into this sprawling structure and form some kind of "islands" of galaxies linked by dark matter "bridges".

After the advent of the COBE and WMAP satellites, the Planck satellite mapped the cosmic microwave background and its minute temperature fluctuations [11]. It allowed us to estimate the ingredients of our Universe. Visible matter contributes just 4.9% of the Universe's energy-mass inventory. Dark matter occupies 26.8%, while dark energy accounts for 68.3%.

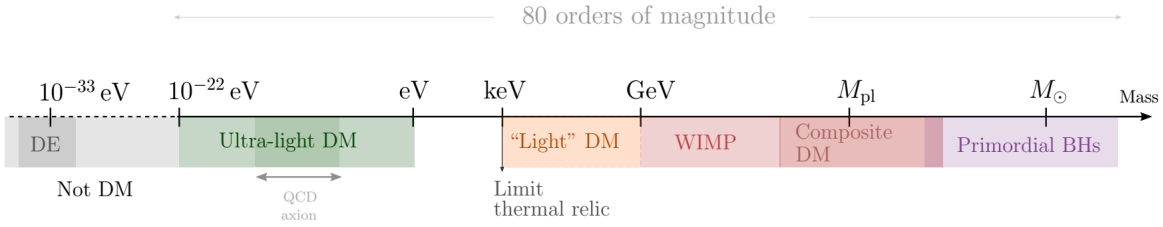

Figure 5: From [22]. Sketch of the range of possible dark matter (DM) models that have been conceived, with dark energy (DE). They span many orders of magnitude in mass, with dark matter candidates, ranging from new elementary particles to black holes.

Gravitational-wave astronomy

September 14, 2015 marked the beginning of a new era in astronomy. On that date, the first-ever direct detection of gravitational waves, ripples of spacetime predicted by Einstein in 1916, took place with the merger of a black hole binary [23][24]. This event GW150914 was produced by the merger of a black hole binary with masses around 36 and 29 solar masses and happened at nearly 1.4 light-years [23]. This detection was possible because the signal is well known and modeled with post-Newtonian techniques, numerical

relativity, and pertubative models. In particular, the merger scenario is the following. A compact binary is made of dense stellar objects such as neutron stars or black holes that orbit each other. The system evacuates part of its energy via gravitational radiation. Therefore, the binary progressively spins up and the compact objects approach each other until coalescence (inspiral phase). It is followed by a phase in which the two objects plunge toward each other, and merge (merger phase). The resulting system, typically a black hole, finally settles down to its ground state, radiating away through vibration modes (ringdown phase). In the case of GW140915, the resulting black hole has 62 solar masses, and the missing mass was radiated away in the form of gravitational radiation [23]. Before the first direction in 2015, scientists suspected the detection of gravitational waves from another event. In 1974, using the Arecibo radio telescope, the Ph.D. student Russel Hulse and his supervisor Joseph Taylor discovered the first binary pulsar PSR B1913+16 [25]. Parameters of their orbit such as the period had been deduced from the Doppler shifting of radio signals. In analogy with a black hole binary, the Hulse-Taylor binary loses energy, and the stars, namely a pulsar and a neutron star, gradually draw closer to each other. A rate of decrease of 2 seconds per year for the 7.75 hours period was expected, but the mechanism was still unknown [25]. Later in 1979, Taylor and Weisberg modeled this decaying period during the inspiral phase via the quadrupolar emission of gravitational waves [26]. It turns out that the model dramatically agrees with the predicted period decrease. It was thus generally accepted as an indirect proof of the existence gravitational waves.
Note that any sources with an accelerating quadrupole produce gravitational waves, including binary inspirals. One of these sources is spinning neutron stars. The latter may exhibit slight deformities on their surface, which are tiny mountains above the stellar surface. This asymmetry gives rise to a varying quadrupole moment during the spinning motion and produces gravitational waves until the deformities are smoothed out [27]. One can also cite core-collapse supernovae for which the spewed-out material has no reason to extend isotropically through the interstellar medium [28]. However, these emission mechanisms are not well understood, and thus suffer from a lack of knowledge about their signal, although the expected strains are in the sensitivity ranges of our current detectors [27][28].

Once gravitational waves cross the Earth, their effect is compressing objects in one direction while simultaneously stretching them in the orthogonal direction (and vice versa). Our Earth-based detectors make use of laser interferometers to detect this deformation pattern. LIGO, Virgo, and KAGRA are inspired by the Michelson configuration. These large-scale interferometers are distinguished by their arms which are several kilometers long. Each arm contains a Fabry-Perot cavity, to artificially increase the optical path (and thus the phase shift). In this way, the laser light travels up to several hundred kilometers within a single arm before recombining on a photodetector. The passage of gravitational waves shrinks the size of one arm while lengthening the other with an oscillating pattern, thus creating a (detectable) phase shift.
On the other hand, resonant bar detectors can also detect gravitational waves but in a narrow frequency band around the resonance frequency. A resonant bar detector is a vibrating system, typically a massive metallic cylinder or sphere, in which a gravitational wave would excite a resonant oscillation. This idea was originally proposed by Joseph Weber in the 1960s with its eponym cylinder [29]. A piezoelectric material is generally glued to the surface to convert the strain into a voltage that can be measured. Since the

resonant frequencies are above 1 kHz, such detectors are more suitable for spinning neutron stars and bursts from type II supernovae. Inspiralling binaries have a considerably lower frequency.

Figure 6: From [30] and [31]. On the left it is an aerial view of the Virgo interferometer located at Cascina near Pisa in Italy. Its arms are 3 km long and the detector operates at frequencies between 20 Hz and 1 kHz. It became operational in 2007. On the right, we have the resonant antenna MiniGRAIL at Leiden University in the Netherlands. Its spherical design allows equal sensitivity in all directions, with a resonnant frequency of 2.9 kHz.

In the future, gravitational wave observations could have an unprecedented impact on several branches of physics, and shed light on phenomena beyond the standard model, in particular dark matter. Many candidates for dark matter exist. Attempting to identify or discriminate them all in a single experiment seems unfeasible and inapropriate, due to their extremely varied properties. This thesis focuses on a particular candidate, and discusses a direct detection method based on an atypical gravitational-wave signature.

Ultra-light scalar cloud

Before starting the thesis, let us get to know the ultra-light scalar cloud. It is rather interesting that we do not observe atoms bound by gravity. A priori, the answer seems rather simple: gravity is weaker than electromagnetism. So, if we want to create a gravitational "atom", we should look at regions where gravity is strong, especially around black holes. A light particle can, in principle, form a bound state with the black hole, while heavier particles would be trapped inside the black hole horizon and thus impossible to detect [32]. In analogy with a conventional atom, these light particles should emit (or absorb) gravitational waves during transitions to lower (or higher) energy levels. In essence, this is a gravitational "atom" with a black hole "nucleus" and a light orbiting particle as the "electron". In addition, it turns out that this light particle could be a dark matter candidate, namely an ultra-light boson. Its mass would be between 10^{-25} eV and 2 eV and adresses the dark matter problem [22]. Detecting a gravitational wave signature from a gravitational atom made of ultra-light bosons would be equivalent to discovering this dark matter particle. Another aspect of the ultra-light bosons that makes these gravitational atoms interesting is that they are not subject to the Pauli exclusion principle. Contrary to the hydrogen atom, the gravitational atom could have an unlimited number of bosons populating each energy level and form a cloud. Gravitational-wave signatures

from the cloud could be transitions, annihilations, or the classical quadrupolar emission during the orbital motion [33][34]. The mechanism to create an ultra-light scalar cloud is the superradiant process and requires spinning black holes, also called Kerr black holes [35].

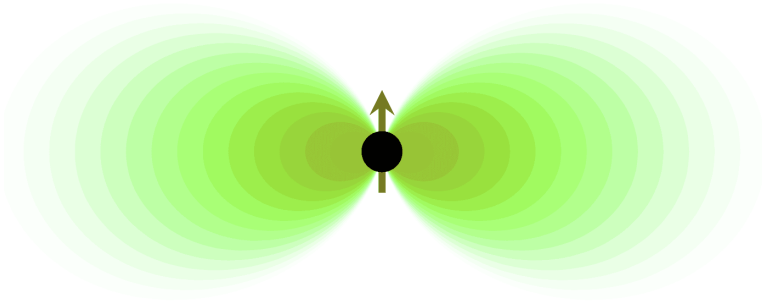

Figure 7: From [36]. Illustration of a gravitational atom with its its scalar cloud (in green) and a spinning black hole (in black), where the arrow indicates the black hole's angular momentum.

Outline

This thesis is divided in four chapters. First, we will overview the main properties of Kerr black holes useful to establish the framework. Then, we will see how to extract rotational energy from the black hole via the superradiance process and how to confine this energy to its surroundings, and thus form a scalar cloud. In chapter 3, we will describe the hydrogen energy spectrum of the cloud and the solutions describing its occupation around the black hole. The dynamics of the cloud will also be discussed. Finally, in the last chapter, we are interested in the emission of gravitational waves due to bosonic transitions within the cloud.

Units and convention

Throughout this thesis we will deal with quantum and astrophysical scales. A convenient unit system is Planck units where $c = \hbar = G = 1$. We can thus get rid of these constants in any equations. All quantities expressible in terms of length, mass, and time in SI units now become dimensionless. Sometimes, we will keep these units when they facilitate the understanding.

Switching from Planck units to SI units (or vice-versa) is possible via this conversion formula

$$\mathrm{m}^{\alpha}\mathrm{kg}^{\beta}\mathrm{s}^{\gamma} = c^{-\frac{(3\alpha-\beta+5\gamma)}{2}}\hbar^{\frac{(\alpha+\beta+\gamma)}{2}}G^{\frac{(\alpha-\beta+\gamma)}{2}}. \tag{1}$$

Rules for converting units for SI to Planck units, and for the reverse conversion, are summarised in the table below. We will adopt the Einstein convention for repeated

Quantity	Planck unit	SI unit
Length	1	$\sqrt{\hbar G/c^3} = 1.61626 \cdot 10^{-35}$m
Mass	1	$\sqrt{\hbar c/G} = 2.176434 \cdot 10^{-8}$kg
Time	1	$\sqrt{G\hbar/c^5} = 5.39125 \cdot 10^{-44}$s
Speed of light in vacuum (c)	1	$2.99792 \cdot 10^{8}$ m s^{-1}
Reduced Planck constant ($\hbar$)	1	$1.05457 \cdot 10^{-34}$ m^2 kg s^{-1}
Cavendish constant (G)	1	$6.67259 \cdot 10^{-11}$ m^3 kg^{-1} s^{-2}

Table 1: Conversion table for Planck units to SI units (or vice-versa) and fundamental constants.

indices in sums, and the spacetime signature [-1, +1, +1, +1], which is typically adopted in General Relativity. Our convention for the indices involved in tensors is the following. Latin indices stand for spatial components (from 1 to 3), and Greek indices run from 0 to 3 (time and space components). The norm of a spacetime vector v^{α} is defined via

$$|| \, v^{\alpha} \, || \equiv g_{\mu\nu}v^{\mu}v^{\nu} \begin{cases} < 0, v^{\mu} \text{ is timelike} \\ = 0, v^{\mu} \text{ is null} \\ > 0, v^{\mu} \text{ is spacelike.} \end{cases} \tag{2}$$

where $g_{\mu\nu}$ is the (covariant) metric tensor. The line element of a metric is expressed in terms of a covariant metric tensor $g_{\mu\nu}$:

$$ds^2 = g_{\mu\nu}dx^{\mu}dx^{\nu}. \tag{3}$$

For instance, the Minkowski spacetime in Cartesian coordinates is written as

$$ds^2 = -dt^2 + dx^2 + dy^2 + dz^2. \tag{4}$$

We will regularly encounter covariant derivatives since the spacetime around black holes is not flat. The covariant derivative of a four-vector with respect to the coordinate x^α is written as

$$\nabla_\alpha v^\mu = \partial_\alpha v^\mu + \Gamma^\mu_{\alpha\lambda} v^\lambda, \tag{5}$$

$$\nabla_\alpha v_\mu = \partial_\alpha v_\mu - \Gamma^\lambda_{\alpha\mu} v_\lambda, \tag{6}$$

where $\partial_\alpha \equiv \frac{\partial}{\partial x^\alpha}$ is the *ordinary* derivative, and $\Gamma^\alpha_{\mu\nu}$ is the Christoffel symbols. The latter vanishes in the Minkowski spacetime. We will also deal with the Levi-Civita connection, which is torsion-free

$$\Gamma^\alpha_{\mu\nu} = \Gamma^\alpha_{\nu\mu}, \tag{7}$$

and metric compatible

$$\nabla_\mu g_{\alpha\beta} = 0. \tag{8}$$

Finally, let us recall the Einstein equations, which take the form

$$R_{\mu\nu} - \frac{1}{2} g_{\mu\nu} R = 16\pi T_{\mu\nu}, \tag{9}$$

where $R_{\mu\nu}$ is the Ricci tensor, R is the Ricci scalar and $T_{\mu\nu}$ is the energy-momentum tensor of the source.

1 | Kerr black holes

In 1915, Albert Einstein proposed the elegant General theory of Relativity [37]. Within two months, Karl Schwarzschild had already found an analytical solution to the field equations of the spacetime geometry for a spherically symmetric mass distribution [38]. Considerably more slowly, only after an intense debate, was it realized that Schwarzschild's solution carries the spacetime manifold representing a static black hole, the endpoint of stellar collapse [39]. However, we know that astrophysical bodies rotate with a given angular momentum. Schwarzschild's solution thus failed to accurately describe such common bodies. No less than 48 years elapsed after the advent of the Schwarzschild solution until the Kerr solution was discovered in 1963 [35]. Physicists and mathematicians looked for such a solution for many years because angular momentum breaks the spherical symmetry and thus makes the calculation much more difficult than previously. Finally, Newman extended this solution to charged rotating mass two years later [40].

In this chapter, we will mainly discuss the properties of rotating black holes, especially the event horizons and the ergoregion, and see how we can extract rotational energy from black holes.

1.1 Kerr-Newman solution

Black holes are formally solutions to Einstein equations admitting an event horizon. Analytic solutions arise from the Einstein equations coupled to Maxwell equations. Our ansatz is summarised in an action

$$S = \frac{1}{16\pi G}\int d^4x\sqrt{-g}\left[R - F_{\mu\nu}F^{\mu\nu}\right], \tag{1.1}$$

with $F_{\mu\nu}$ the electromagnetic field strength tensor, R the Ricci scalar, and $g = det(g_{\mu\nu})$. The associated equations of motion are given by

$$\begin{aligned} &R_{\mu v} - \tfrac{1}{2}g_{\mu v}R = 2\left(F_{\mu\lambda}F_{v}^{\lambda} - \tfrac{1}{4}g_{\mu\nu}F_{\lambda p}F^{\lambda p}\right), \\ &\nabla_{\mu}F^{\mu\nu} = 0, \end{aligned}$$

where $R_{\mu\nu}$ is the Ricci tensor and ∇_{μ} the covariant derivative [41]. An axially symmetric solution for the metric is known as the Kerr-Newman metric [40]. The explicit form of

the Kerr-Newmann metric is [41]

$$ds^2 = \left(1 - \frac{2Mr}{\rho^2}\right) dt^2 + \frac{4aMr\sin^2\theta}{\rho^2} dt d\phi - \frac{\rho^2}{\Delta} dr^2 - \rho^2 d\theta^2 - \left[\left(r^2 + a^2\right)\sin^2\theta + \frac{2Mr}{\rho^2} a^2 \sin^4\theta\right] d\phi^2 \tag{1.2}$$

where

$$\rho^2 \equiv r^2 + a^2\cos^2\theta \text{ and } \Delta \equiv r^2 - 2Mr + a^2 + Q^2, \tag{1.3}$$

while the inverse metric tensor $g^{\mu\nu}$ is defined by

$$g^{\mu\nu} = \begin{pmatrix} -\frac{1}{\Delta}[r^2 + a^2 + \frac{2Mra^2}{\rho^2}\sin^2\theta] & 0 & 0 & -\frac{2Mra}{\rho^2\Delta} \\ 0 & \frac{\Delta}{\rho^2} & 0 & 0 \\ 0 & 0 & \frac{1}{\rho^2} & 0 \\ -\frac{2Mra}{\rho^2\Delta} & 0 & 0 & \frac{\Delta - a^2\sin^2\theta}{\Delta\rho^2\sin^2\theta} \end{pmatrix}. \tag{1.4}$$

The three parameters are the mass M, the charge Q, and the angular momentum $J = aM$ of the black hole, where a is the angular momentum per unit mass. Without loss of generality, one can assume a positive spin-mass ratio a. Coordinates $\{t, r, \theta, \phi\}$ are called Boyer-Lindquist coordinates. We have a temporal coordinate t in which everything is stationary, ϕ is the angle around the spin axis, a "radial" coordinate r, and another "angular" coordinate θ. The Kerr-Newmann solution for the Maxwell potential is

$$A_\mu dx^\mu = \frac{Qr\left(dt - a\sin^2\theta d\phi\right)}{\rho^2}. \tag{1.5}$$

The Kerr-Newmann metric describes the spacetime of the most general black holes of mass M, spinning with an angular momentum J, and carrying an electric charge Q. It is quite surprising that whatever the process through which black holes are formed, they are described by only three parameters. It is often said that black holes have "no hair", or are "bald", in the sense that they are hardly differentiated.

In the following, we will set the charge $Q = 0$. This assumption allows us to simplify the metric and is motivated by the negligible effect of the charge on the metric [42]. Such metric is called the Kerr metric, and neutral spinning black holes are called Kerr black holes [35]. Some properties of the Kerr spacetime can be deduced from the line element (1.3):

(i) Since the metric components do not depend on t and ϕ, the Kerr spacetime admits both Killing vectors $\xi^\alpha = \partial_t$ and $\psi^\alpha = \partial_\phi$ (cf. appendix [A] for a brief introduction to Killing vectors). The Kerr spacetime is stationary and axially symmetric. However, since the time reflection $t \to -t$ is not a symmetry, the Kerr spacetime cannot be static.

(ii) In the non-rotating limit $a \to 0$, the Kerr spacetime reduces to the Schwarzschild spacetime.

(iii) If $r \to \infty$, the Kerr spacetime reduces to the Minkowski spacetime in polar coordinates. The Kerr spacetime is said to be asymptotically flat.

1.2 Coordinate systems

In addition to the Boyer-Linquist coordinates $\{t, r, \theta, \phi\}$, we will work with two other coordinate systems for the Kerr spacetime, since some coordinates are more appropriate to certain situations. Depending on the framework, we will thus specify the coordinates that will be used. Before starting the discussion, a brief overview of each coordinate system is presented in the Table 1.1.

	Boyer-Lindquist	Kerr-Schild	Ingoing-Kerr
Coordinates	t, r, θ, ϕ	$\bar{t}, x, y, z$	$\tilde{t}, r, \theta, \tilde{\phi}$
Metric tensor	$g_{\mu\nu}$	$\bar{g}_{\mu\nu}$	$\tilde{g}_{\mu\nu}$
Advantages	Only two off -diagonal terms	$r = cst$ surfaces are oblate spheroids	Regularity at $r = r_+$

Table 1.1: A brief overview of each coordinate system.

1.2.1 Kerr-Schild coordinates

The natures of the singularity and other peculiar surfaces are best seen in the Cartesian Kerr-Schild coordinates [43]. In the Kerr-Schild coordinate system $\left\{\bar{t}, x, y, z\right\}$, with the usual spatial Cartesian coordinates $\{x, y, z\}$, the Kerr spacetime is decomposed into perturbations to Minkowski spacetime. Its line element is written as [43]

$$\begin{aligned} \mathrm{d}s^2 = &-\mathrm{d}\bar{t}^2 + \mathrm{d}x^2 + \mathrm{d}y^2 + \mathrm{d}z^2 \\ &+ \frac{2mr^3}{r^4 + a^2z^2}\left[\mathrm{d}\bar{t} + \frac{r(x\ \mathrm{d}x + y\ \mathrm{d}y)}{a^2 + r^2} + \frac{a(y\ \mathrm{d}x - x\ \mathrm{d}y)}{a^2 + r^2} + \frac{z}{r}\ \mathrm{d}z\right]^2. \end{aligned} \tag{1.6}$$

The Kerr-Schild coordinates $\{\bar{t}, x, y, z\}$ are related to the Boyer-Lindquist coordinates $\{t, r, \theta, \phi\}$ via the following relations [41]

$$x + iy = (r + ia)\sin\theta \exp\left[i\int\left(d\phi + \frac{a}{\Delta}dr\right)\right], \tag{1.7}$$

$$z = r\cos\theta, \tag{1.8}$$

$$\bar{t} = \int\left(dt + \frac{r^2 + a^2}{\Delta}dr\right) - r, \tag{1.9}$$

which imply that the function $r = r(x, y, z)$ is implicitly defined via

$$\frac{x^2 + y^2}{r^2 + a^2} + \frac{z^2}{r^2} = 1. \tag{1.10}$$

The surfaces of constant r are thus oblate spheroids, i.e. ellipsoids of revolution for which the semi-minor axis is along the z-axis. Equation (1.10) allows one to draw diagrams of specific regions of the Kerr spacetime. Indeed, if one sets $x = 0$ and uses (1.8), relation (1.10) becomes

$$y = \sqrt{r^2 + a^2}\sin\theta. \tag{1.11}$$

If we combine this relation with (1.8), we can then easily make plots in the plane $x = 0$.

1.2.2 Ingoing-Kerr coordinates

A deficiency of the Boyer-Lindquist coordinate system is that it takes an infinite coordinate time t for ingoing geodesics to reach the outer event horizon. A more physically realistic coordinate system is the ingoing-Kerr coordinate system $\left\{\tilde{t}, r, \theta, \tilde{\phi}\right\}$, which is defined by [44]

$$d\tilde{t} = dt + \frac{2Mr}{\Delta} dr, \tag{1.12}$$

and

$$d\tilde{\phi} = d\phi + \frac{a}{\Delta} dr. \tag{1.13}$$

The r and θ coordinates are identical in both coordinate systems. Explicitly, the new coordinates are related by

$$\tilde{t} = t + \alpha(r) \quad \tilde{\phi} = t + \beta(r), \tag{1.14}$$

where

$$\alpha(r) = \frac{2Mr_+}{r_+ - r_-} \ln|r - r_+| - \frac{2Mr_-}{r_+ - r_-} \ln|r - r_-|, \tag{1.15}$$

$$\beta(r) = \frac{a}{r_+ - r_-} \ln\left|\frac{r - r_+}{r - r_-}\right|. \tag{1.16}$$

The event horizons are now perfectly regular in our metric, and there are no coordinate singularities as is the case with the Boyer-Lindquist system. In this coordinate system, the inverse metric takes a simple form

$$\tilde{g}^{\mu\nu} = \frac{1}{\rho^2} \begin{pmatrix} -(\rho^2 + 2Mr) & 2Mr & 0 & 0 \\ 2Mr & \Delta & 0 & a \\ 0 & 0 & 1 & 0 \\ 0 & a & 0 & \frac{1}{\sin^2\theta} \end{pmatrix}. \tag{1.17}$$

1.3 Metric singularities

Our Kerr metric in Boyer-Lindquist coordinates (1.2) is singular for $\Delta = 0$ and $\rho^2 = 0$. We will see that these quadratic equations identify two types of singularities. Let us first focus on the quadratic equation

$$\rho^2 \equiv r^2 + a^2 \cos^2\theta = 0. \tag{1.18}$$

A real solution appears for $r = 0$ and $\theta = \pi/2$. If we evaluate the Ricci scalar at the coordinates defined by $r = 0$ and $\theta = \pi/2$, the curvature scalar tends towards infinity. In other words, the real solution identifies a curvature singularity. Its shape is easily understood by considering the Kerr-Schild coordinates. Indeed, in this (Cartesian) coordinate system, the curvature singularity is defined via

$$x^2 + y^2 = a^2, \tag{1.19}$$

with $z = 0$. The singularity is thus a ring of radius a in the plane $z = 0$. In the limit of a static black hole $a \to 0$, the ring singularity reduces to a point-like singularity, as is the case for a Schwarzschild black hole.

Now, let us see that the quadratic equation $\Delta = 0$ identifies a coordinate singularity, and especially two event horizons. This polynomial equation for r can be written as

$$\Delta \equiv r^2 - 2Mr + a^2 = (r - r_+)(r - r_-), \tag{1.20}$$

where $r_\pm \equiv M \pm \sqrt{M^2 - a^2}$ are real roots if $M^2 > a^2$. If $M^2 < a^2$, we do not have any real roots. The ring singularity would not be screened by any event horizons, and we would have a "naked" singularity. This case is not allowed by the cosmic censorship conjecture, which assumes that all singularities must be screened by a horizon. The case $M^2 < a^2$ will thus be considered all along the thesis, and implies that $a = M$ is the maximal angular momentum per unit mass of a black hole.
Consider now the hypersurfaces $f(x^\mu) = r$, for which the normal vector is given by

$$\partial_\alpha r = [0, 1, 0, 0], \tag{1.21}$$

while its norm is

$$||\partial_\alpha r\,|| \equiv g^{\mu\nu}\partial_\mu r \partial_\nu r = g^{rr} = \frac{\Delta}{\rho^2}. \tag{1.22}$$

In the limit $r \to r_\pm$, the normal vector $\partial_\alpha r$ becomes null. The null hypersurfaces $r = r_\pm$ are thus event horizons. In particular, we have an outer event horizon $r = r_+$ and an inner event horizon $r = r_-$, since $r_+ > r_-$. Causal implications for an observer that crosses both event horizons are rather exotic and disturbing. A detailed discussion requires the use of Penrose diagrams and the introduction of new mathematical tools. However, it appears that the inner event horizon is actually not physically relevant since it seems to be unstable with respect to gravitational perturbations and unlikely to form in any real astrophysical collapse [45]. Unless otherwise specified, we will thus solely consider the outer event horizon, and call it "the event horizon".

1.4 Ergoregion

A surprising feature of the Kerr spacetime is a region in the vicinity of the black hole where no observer can remain static. It is commonly called the ergoregion. As we will see later, this atypical region allows extracting energy from a black hole. To introduce it, consider the Killing vector ξ^α. The latter does not need to be timelike everywhere since its norm in the Boyer-Lindquist system is

$$\xi^\alpha \xi_\alpha = g_{tt} = -\left(1 - \frac{2Mr}{r^2 + a^2\cos^2\theta}\right). \tag{1.23}$$

Thus, ξ_α is spacelike provided that

$$r^2 + a^2\cos^2\theta - 2Mr < 0. \tag{1.24}$$

Since the spin-mass ratio is constrained by $a^2 > M^2$, the Killing vector ξ^α is *spacelike* in the region outside the event horizon defined by

$$r_+ < r < r_{s+}, \tag{1.25}$$

where $r_{s+} \equiv M + \sqrt{M^2 - a^2 \cos^2 \theta}$ is the larger root of the polynomial in (1.24). This region (1.25) is called the ergoregion, and its boundaries form the ergosphere. Note that ξ^α is also spacelike for

$$r_{s-} < r < r_+, \tag{1.26}$$

where $r_{s-} \equiv M - \sqrt{M^2 - a^2 \cos^2 \theta}$ is the other root of the polynomial in (1.24). However, since this region is inside the outer event horizon, we can neglect it. Consider now a timelike world line for an observer, a clock attached to him of her with a proper time τ, and u^μ the four-velocity, or the tangent vector to this timelike word line. Hence, since it is timelike, the norm of the tangent vector u^μ verifies everywhere

$$g_{\mu v} u^\mu u^v < 0. \tag{1.27}$$

Inside the ergosphere, all terms on the left-hand side are positive except the term $2g_{t\phi}u^t u^\phi$. Thus, since $g_{t\phi} < 0$ and $u^t > 0$ in the ergosphere, any timelike curve must verify

$$u^\phi = \frac{d\phi}{d\tau} > 0 \tag{1.28}$$

In other words, all observers in the ergoregion are dragged and co-rotates with the black hole. Contrary to an event horizon, this is not a "no escape region" and observers may leave the ergoregion after they enter it.

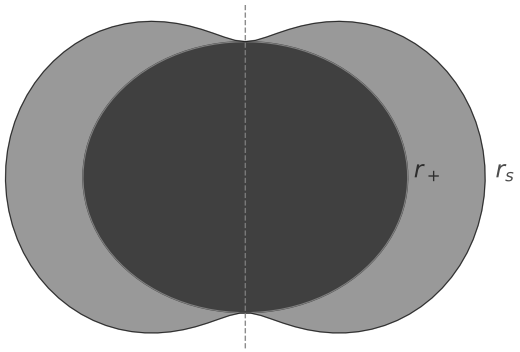

Figure 1.1: Slice in the plane $x = 0$ of the stationary surface $r_s = M + \sqrt{M^2 - a^2 \cos^2 \theta}$, and the event horizon $r_+ = M + \sqrt{M^2 - a^2}$ in Kerr-Schild coordinates. The ergoregion (in grey) is between r_s and r_+. The dashed lines represent the spin axis of the black hole (in black). If its spin tends towards zero, $a \to 0$, these surfaces coincide.

1.5 Angular velocity of the event horizon

Defining an angular velocity in our framework is much more abstract than in the Newtonian case. The angular velocity of the event horizon plays an important role in the superradiance process. A natural way to introduce this angular velocity is to consider that a massive particle moves in the ϕ direction in the equatorial plane $\theta = \pi/2$ at a time t. Since at this moment its momentum has no component in the radial r and the angular θ directions, the motion of the particle is constrained by

$$ds^2 = g_{tt}dt^2 + 2g_{t\phi}d\phi dt + g_{\phi\phi}d\phi^2 < 0, \tag{1.29}$$

By dividing this relation by dt^2, we get a quadratic inequality for $d\phi/dt$. We can rewrite this inequality as

$$\Omega_0 < \frac{\mathrm{d}\phi}{\mathrm{d}t} < \Omega_1 \tag{1.30}$$

where

$$\Omega_{0,1} = -\frac{g_{t\phi}}{g_{\phi\phi}} \pm \sqrt{\left(\frac{g_{t\phi}}{g_{\phi\phi}}\right)^2 - \frac{g_{tt}}{g_{\phi\phi}}}. \tag{1.31}$$

Now, suppose that the massive particle enters inside the ergosphere, where g_{tt} is null. In the limit as the particle approaches the black hole event horizon, $r \to r_+$, its minimal coordinate angular velocity Γ_0 becomes

$$\Omega_H \equiv \Omega_0(r_+) = \frac{a}{r_+^2 + a^2} = \frac{a}{2Mr_+}. \tag{1.32}$$

Hence, the angular velocity of the event horizon, noted Ω_H, is defined as the minimum angular velocity of a massive particle at the horizon.

1.6 Penrose process

A black hole is a region where "nothing can escape", even a light ray or a material body [46]. In 1969, Penrose noted that it is actually possible to extract energy from a black hole if it spins [47]. This mechanism, known as the Penrose process, is analogous to black hole superradiance, but for particles. To understand it, consider a massive particle that follows a geodesic in the vicinity of a rotating black hole. Its four-momentum is simply

$$p^\mu = m\frac{dx^\mu}{d\tau} \tag{1.33}$$

with m its rest mass. Previously, we have seen that the Kerr metric possesses the Killing vectors $\xi^\alpha = \partial_t$ and $\psi^\alpha = \partial_\phi$. One can associate a conserved quantity with a Killing vector (cf. Appendix A for explanations). In the Kerr spacetime, the energy of a particle

E and its angular momentum L are conserved, respectively

$$E = -\xi^\mu p_\mu = m\left(1 - \frac{2Mr}{\rho^2}\right)\frac{dt}{d\tau} + \frac{8Mmar}{\rho^2}\sin^2\theta\frac{d\phi}{d\tau}, \tag{1.34}$$

$$L = \psi^\mu p_\mu = -\frac{8Mmar}{\rho^2}\sin^2\theta\frac{dt}{d\tau} + \left(r^2 + a^2\right)\sin^2\theta + \frac{2Mr}{\rho^2}a^2\sin^4\theta\frac{d\phi}{d\tau}. \tag{1.35}$$

The Killing vector ξ^μ becomes spacelike in the ergosphere. Thus, for a test particle in the ergosphere, the energy can be negative. Suppose now that the particle decays into two others in the ergosphere, one of which falls into the black hole while the other escapes to infinity. At the moment the particle decays, energy is locally conserved

$$E_2 = E_0 - E_1, \tag{1.36}$$

with E_0 the initial energy (cf. Figure 1.2). Since ξ^μ is spacelike inside the ergoregion, the energy E_1 of the particle falling into the black hole may be negative. Thus, the energy E_2 can be greater than the initial energy. Energy does not come from anywhere but has been extracted by decreasing the angular momentum of the black hole.

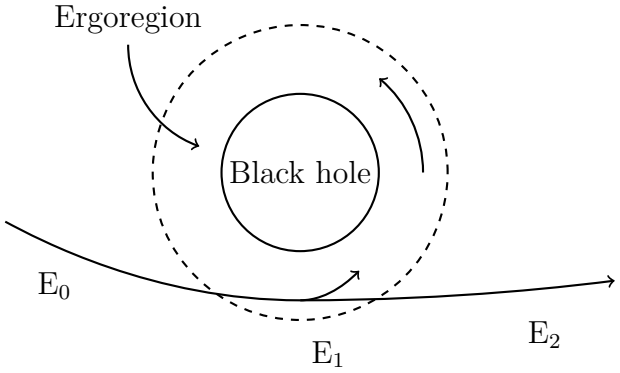

Figure 1.2: Illustration of the Penrose process (top view).

To understand how the energy is extracted from the black hole, consider a new Killing vector formed by making a linear combination with ξ^μ and ψ^μ

$$\chi^\mu = \xi^\mu + \Omega_H\psi^\mu, \tag{1.37}$$

where Ω_H is the angular velocity of the event horizon (1.32). For any particle which crosses the (outer) event horizon at $r = r_+$, we have

$$\chi^\mu p_\mu < 0. \tag{1.38}$$

Plugging the definitions of E (1.29) and L (1.30) into this condition yields

$$L < \frac{E}{\Omega_H}. \tag{1.39}$$

Hence, a negative energy particle carries a negative angular momentum, i.e. the particle moves *against* the black hole's rotation. Once a negative-energy particle crosses the event

horizon, we end up with a black hole mass $M + \delta M$ and an angular momentum $J + \delta J$, where $\delta M = E$ and $\delta J = L$. Therefore, the angular momentum of the black hole decreases as long as negative energy particles cross the event horizon. When the black hole is no longer spinning, its ergoregion disappears and the Penrose process ends. However, note that any particle can enter the event horizon, including positive energy particles. The mass and the angular momentum of the black hole are thus not necessarily decreasing during its evolution.

2 | Massive scalar field on a Kerr background

This chapter is dedicated to the superradiant instability of a spinless massive boson field in the Kerr spacetime. First, we will introduce the formalism for a scalar field in curved spacetime. Then, we will see how we can extract energy from a wave packet entering a black hole. Finally, we will discuss under which conditions a massive scalar field can form unstable bound states around a rotating black hole.

2.1 Formalism for scalars in Kerr spacetime

We consider spinless massive charged bosons in the vicinity of a Kerr black hole. Hence, we must couple the Klein-Gordon field to gravity, in particular to the Kerr spacetime. In a Minkowski spacetime, the Lagrangian density of a scalar field is given by [48]

$$\mathcal{L} = \frac{1}{2} g^{\alpha\beta} \partial_\alpha \Phi^* \partial_\beta \Phi - \frac{1}{2} \mu^2 |\Phi|^2, \tag{2.1}$$

where μ is the mass of the spinless particle, and Φ^* is the complex conjugate of the field Φ. The basic procedure for the gravitational coupling is to substitute the Minkowski metric with the Kerr metric, and ordinary derivatives with covariant derivatives, i.e.

$$\partial_\mu \mapsto \nabla_\mu. \tag{2.2}$$

In addition, one can also add a coupling term to the Ricci scalar R. Finally, we end up with the following Lagrangian density[1]

$$\mathcal{L} = \frac{1}{2} g^{\alpha\beta} \nabla_\alpha \Phi^* \nabla_\beta \Phi - \frac{1}{2} \mu^2 |\Phi|^2 - \chi |\Phi|^2 R, \tag{2.3}$$

and its action

$$S = \int d^4x \sqrt{-g}\, \mathcal{L}, \tag{2.4}$$

[1] Ordinary derivatives and covariant derivatives are equivalent when they applied to a scalar quantity, which means that $\partial_\mu \Phi = \nabla_\mu \Phi$ and $\partial^\mu \Phi = \nabla^\mu \Phi$. However, $\partial^\mu(\partial_\mu \Phi)$ is strictly different from $\nabla^\mu(\partial_\mu \Phi)$ since the second derivative is no longer applied to a scalar quantity, but a vectorial quantity $\partial_\mu \Phi$.

with χ a dimensionless coupling constant to the Ricci scalar. In the literature, there are two favorite choices for the value of χ. Conformal coupling sets

$$\chi = \frac{(n-2)}{4(n-1)}, \tag{2.5}$$

with n the dimension of spacetime. For example, $\chi = \frac{1}{6}$ in four dimensions. On the other hand, minimal coupling turns off the direct interaction with R,

$$\chi = 0. \tag{2.6}$$

Conformal coupling is used if one wants to build a theory invariant under conformal transformations $g_{\mu\nu} \to \omega^2(x) g_{\mu\nu}$. In our framework, such symmetry is certainly not useful. One may thus opt for minimal coupling and delete the coupling term in our Lagrangian density (2.3).

Varying the action (2.4) with respect to the field yields the equation of motion of a massive charged scalar field Φ around a rotating black hole

$$\left(\Box - \mu^2\right) \Phi = 0, \tag{2.7}$$

where $\Box \equiv g^{\alpha\beta} \nabla_\alpha \nabla_\beta$ is the d'Alembertian, and $g_{\alpha\beta}$ is the Kerr metric. This equation of motion (2.7) is analoguous to the typical Klein-Gordon equation in flat spacetime, except that ordinary derivatives are just replaced by covariant derivatives.

A scalar field in a Kerr background is separable due to the axisymmetry of the Kerr spacetime, which makes our problem analytically tractable. Tensor fields and vectors are not separable in the Kerr spacetime [49]. In Boyer-Lindquist coordinates $\{t, r, \theta, \phi\}$, the field is separable into [49]

$$\Phi(t, r, \theta, \phi) = e^{im\phi - i\omega t} S(\theta) R(r), \tag{2.8}$$

where $m \in \mathbb{Z}$ is the azimuthal number, and ω is a (complex) frequency. The real part $\mathrm{Re}(\omega)$ corresponds to the frequency of the field, or of the wave packet, and the imaginary part $\mathrm{Im}(\omega)$ is the rate at which the perturbation grows or decays with time. Therefore, from (2.8), the field is decaying if $\mathrm{Im}(\omega) < 0$, and amplified if $\mathrm{Im}(\omega) > 0$.
Since the field is scalar, it is invariant with respect to a change of coordinates. The radial functions in ingoing-Kerr coordinates are hence given by

$$\tilde{R}(r) = e^{im\tilde{\phi}} e^{-i\omega\tilde{t}} R(r). \tag{2.9}$$

2.2 Superradiance process

Consider a scalar wave incident upon a Kerr black hole. Part of the wave will be absorbed by the black hole and part of the wave will escape back to infinity. In the superradiant regime, the transmitted wave will carry negative energy into the black hole, which is analogous to the negative energy particle in the Penrose process, and the reflected wave will return to infinity with greater energy than the incident wave. In this section, we will demonstrate this effect, and show how it could create unstable bound states around a Kerr black hole. The derivation is inspired by [50].

2.2.1 Conserved quantities

Several useful quantities are conserved. By varying the action (2.4) with respect to the metric, one obtains the symmetric stress-energy tensor of a minimally coupled, complex, spinless, massive scalar field

$$T^{\mu}{}_{\nu} = \frac{1}{2}\left(\nabla^{\mu}\Phi^{*}\nabla_{\nu}\Phi + \nabla_{\nu}\Phi^{*}\nabla^{\mu}\Phi\right) - \delta^{\mu}{}_{\nu}\mathcal{L}. \tag{2.10}$$

Note that one could use ordinary derivatives instead of covariant derivatives involved in the stress-energy tensor, as they act on scalar quantities. The stress-energy tensor is conserved since it satisfies the conservation law $\nabla_{\mu}T^{\mu}{}_{\nu} = 0$ (cf. Appendix B for details). One can form a four-current J^{ν} by contracting the stress-energy tensor with the Killing field $\xi^{\alpha} = [1, 0, 0, 0]$ conjugate to the time coordinate :

$$J^{\mu} = -\xi^{\alpha}T^{\mu}{}_{\alpha} = -T^{\mu}{}_{0}. \tag{2.11}$$

This current may be interpreted as an energy four-current. It is not to be confused with the electric four-current of a charged Klein-Gordon field. The conservation law of the stress-energy tensor $\nabla_{\mu}T^{\mu}{}_{\nu} = 0$ and Killing's equation $\nabla_{\mu}\xi_{\nu} + \nabla_{\nu}\xi_{\mu} = 0$ (cf. Appendix A for details) yield a conserved current

$$\nabla_{\nu}J^{\nu} = -\left(\nabla_{\nu}\xi_{\mu}\right)T^{\mu\nu} - \xi_{\mu}(\nabla_{\nu}T^{\mu\nu}) = 0. \tag{2.12}$$

2.2.2 Time evolution of the field

Now, we have all the tools required to relate the energy flux of the field across the event horizon to its energy outside the black hole. We will use the ingoing-Kerr coordinate system $\{t, r, \theta, \phi\}$ since the latter is not singular at the event horizon. From the divergence-free current one get a conservation law via Gauss's theorem [51],

$$\int_{\mathcal{V}} d^{4}x\, \nabla_{\mu}J^{\mu} = \int_{\partial\mathcal{V}} d^{3}x\, n_{\mu}J^{\mu} = 0, \tag{2.13}$$

where $\mathcal{V}$ is a four-volume and its boundary $\partial\mathcal{V}$, and n_{μ} is an outward-pointing normal to the boundary $\partial\mathcal{V}$. We construct a four-volume $\mathcal{V}$ of width $\Delta\tilde{t}$ bounded by an upper spacelike hypersurface Σ_2 ($\tilde{t} = \tilde{t}_0 + \Delta\tilde{t}$, $r > r_+$) and a lower hypersurface Σ_1 ($\tilde{t} = \tilde{t}_0$, $r > r_+$), and a null hypersurface $\mathcal{N}$ at the event horizon ($r = r_+, \tilde{t}_0 < \tilde{t} < \tilde{t}_0 + \Delta\tilde{t}$). Applying the conservation law (2.13) to this four-volume $\mathcal{V}$ and assuming the four-current vanishes at spatial infinity, i.e. if $\nabla_{\mu}\Phi = 0$, gives

$$\int_{\Sigma_2} d^{3}x\, n^{2}_{\mu}J^{\mu} - \int_{\Sigma_1} d^{3}x\, n^{1}_{\mu}J^{\mu} + \int_{\mathcal{N}} d^{3}x\, k_{\mu}J^{\mu} = 0 \tag{2.14}$$

with n^{i}_{μ} and k_{μ} normal vectors to Σ_i and $\mathcal{N}$. The first term and the second term are respectively the outgoing energy and the ingoing energy of the scalar wave. The last integral corresponds to the energy flux through the event horizon. Now, imagine that we bring infinitesimally closer the hypersurfaces Σ_1 and Σ_2. Taking the limit $\Delta\tilde{t} \to 0$ and

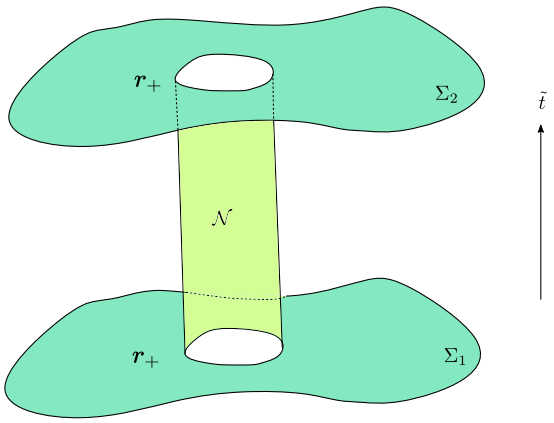

Figure 2.1: Sketch of the boundary of our four-volume $\mathcal{V}$, with $\partial\mathcal{V} = \Sigma_1 \cup \Sigma_2 \cup \mathcal{N}$. The intersection between the null hypersurface $\mathcal{N}$ and the spacelike hypersurfaces Σ_1 and Σ_2 is a static view of the event horizon.

rearranging the terms, leads to a quasi-local conservation law for the energy

$$\frac{\partial}{\partial\tilde{t}}\left\{\int_\Sigma d^3x\, n_\mu J^\mu\right\} = -\int_\mathcal{N} d^2x\, k_\mu J^\mu, \tag{2.15}$$

where the right-hand side's integral is now only over space, so that the integration element becomes d^2x instead of d^3x. The surfaces $\mathcal{N}$ and Σ and normal vectors n_μ and k_μ are now defined by

$$\mathcal{N}: \quad \tilde{t} = \tilde{t}_0, r = r_+, \quad k_\mu = -\delta^1_\mu, \tag{2.16}$$
$$\Sigma: \quad \tilde{t} = \tilde{t}_0, r > r_+, \quad n_\mu = \delta^0_\mu/\tilde{g}^{00}. \tag{2.17}$$

To calculate the integrals (2.15), we inject our ansatz (2.8) for the field into the four-current (2.11). One may note that the integration elements d^3x and d^2x are not as simple as a classical integration in $\mathbb{R}^n$. Indeed, we have [51]

$$d^3x = \sqrt{|\gamma_\Sigma|}\, dr d\theta d\tilde{\phi}, \quad d^2x = \sqrt{|\gamma_\mathcal{N}|}\, d\theta d\tilde{\phi}, \tag{2.18}$$

where $\gamma = \det(\gamma_{ij})$ and γ_{ij} are the components of the induced metric onto the surface Σ or $\mathcal{N}$. The integral of the left-hand side of (2.15) involves a time-derivative of the energy density of the field. After some algebraic manipulations, the local conservation law (2.15) becomes

$$2\,\mathrm{Im}(\omega)\int_\Sigma d^3x\, J^0 = -\int_\mathcal{N} d^2x\, k_\mu J^\mu. \tag{2.19}$$

On the other hand, the surface integral of the right-hand side is straightforward to compute since our metric is expressed in terms of angular coordinates. Indeed, computing the induced metric leads to

$$\begin{aligned}\int_\mathcal{N} d^2x\, k_\mu J^\mu &= -\int_\mathcal{N} d^2x\, J^1, \\ &= -\int_0^\pi\int_0^{2\pi} d\theta d\tilde{\phi}\, \rho^2 \sin\theta\, J^1,\end{aligned} \tag{2.20}$$

while, from (2.10) and (2.11), the radial component of the current at the event horizon is

$$J^1 = -\frac{1}{\rho^2}\left(2Mr_+|\omega|^2 - am\,\mathrm{Re}(\omega)\right)|S(\theta)|^2\left|\tilde{R}\,(r_+)\right|^2. \tag{2.21}$$

Consequently, the integral (2.20) becomes

$$\int_{\mathcal{N}} d^2x\; k_\mu J^\mu = 2\pi\left(2Mr_+|\omega|^2 - am\,\mathrm{Re}(\omega)\right)\left|\tilde{R}\,(r_+)\right|^2\int_0^\pi d\theta\,|S(\theta)|^2\sin\theta. \tag{2.22}$$

Assuming the angular function $S(\theta)$ is normalised to $\int_0^\pi d\theta|S(\theta)|^2\sin\theta = 1/(2\pi)$, our local conservation law (2.15) thus translates into a relation for the complex frequency:

$$2\,\mathrm{Im}(\omega) = \left(2Mr_+|\omega|^2 - am\,\mathrm{Re}(\omega)\right)\frac{\left|\tilde{R}\,(r_+)\right|^2}{\int_\Sigma d^3x\;J^0}. \tag{2.23}$$

The energy density of the field J^0 is positive everywhere outside the ergoregion, but it could be negative within this region since the Killing field ξ^α becomes spacelike. One may assume that the integral involving J^0 in (2.23) is non zero and positive, otherwise, a change of sign of $\mathrm{Im}(\omega)$ would lead to an infinite growth rate. This has not been observed during various numerical simulations [50] so we can assume J^0 is non zero and positive. Finally, the field is growing in time if $\mathrm{Im}(\omega) > 0$, i.e. if

$$\frac{|\omega|^2}{\mathrm{Re}(\omega)} < m\,\Omega_H, \tag{2.24}$$

with $\Omega_H = \frac{a}{2Mr_+}$ the angular velocity of the event horizon (1.32). In particular, if $|\,\mathrm{Re}(\omega)| \gg |\,\mathrm{Im}(\omega)|$, the latter equation reduces to the well-known superradiance condition

$$\mathrm{Re}(\omega) < m\,\Omega_H. \tag{2.25}$$

If an incident wave onto the event horizon is in the superradiance regime (2.25), rotational energy is extracted from the black hole and used to get a reflected wave with an energy higher than the incident one. This is the superradiant scattering [52], which may also affect electromagnetic waves and gravitational waves [46]. If the black hole is not sufficiently spinning, energy cannot be extracted, even if the ergoregion is still present. This marks a radical difference from the Penrose process, which allows energy extraction only if the black hole spins.

A rather interesting consequence could arise from the superradiance condition (2.25). Imagine a wave packet of a massive scalar field bound to the black hole in an orbit. The gravitational force binds the field and keeps it from escaping or radiating away to infinity. Some of the field goes down the black hole at the event horizon, and if the frequency of the field satisfies condition (2.24), then the field can be amplified at the event horizon while being bound on an orbit. The mass of the field acts as a natural mirror [52] that reflects amplified waves towards the event horizon, which are amplified again via the superradiance scattering, etc... This cumulative effect opens up the existence of unstable bound states. In the following section, we will see that unstable bound states are indeed possible.

2.3 Klein-Gordon equation

2.3.1 Separation

A massive scalar field in a Kerr spacetime obeys the wave equation (2.7). A major difficulty of this equation is that it involves covariant derivatives. However, we can circumvent this difficulty by using the famous formula [51]

$$\nabla_\mu(\nabla^\mu\Phi) = \frac{1}{\sqrt{-g}}\partial_\mu(\sqrt{-g}\,\nabla^\mu\Phi),$$

with $g = \det(g_{\mu\nu})$. Using this formula for the Klein-Gordon equation (2.7) allows one to write it only in terms of ordinary derivatives

$$\frac{1}{\sqrt{-g}}\partial_\mu\left(\sqrt{-g}g^{\mu\nu}\partial_\nu\Phi\right) + \mu^2\Phi = 0. \tag{2.26}$$

In Boyer-Lindquist coordinates, the latter equation takes the following form [50]

$$\left(\frac{\left(r^2+a^2\right)^2}{\Delta} - a^2\sin^2\theta\right)\partial_t\partial_t\Phi + \frac{4mar}{\Delta}\partial_t\partial_\phi\Phi + \left(\frac{a^2}{\Delta} - \frac{1}{\sin^2\theta}\right)\partial_\phi\partial_\phi\Phi$$
$$-\partial_r\left(\Delta\partial_r\Phi\right) - \frac{1}{\sin\theta}\partial_\theta\left(\sin\theta\partial_\theta\Phi\right) + \mu^2\rho^2\Phi = 0. \tag{2.27}$$

This differential equation may look scary. Nevertheless, we should remember our ansatz (2.8) for the field. Injecting it into the wave equation allows us to split it into two differential equations. Therefore, we get an angular equation

$$\frac{1}{\sin\theta}\frac{d}{d\theta}\left(\sin\theta\frac{dS}{d\theta}\right) + \left[a^2\left(\omega^2-\mu^2\right)\cos^2\theta - \frac{m^2}{\sin^2\theta} + \Lambda\right]S(\theta) = 0, \tag{2.28}$$

and a radial equation

$$\Delta\frac{d}{dr}\left(\Delta\frac{dR}{dr}\right) + \left[\omega^2\left(r^2+a^2\right)^2 - 4Mam\omega r + m^2a^2 - \Delta\left(\omega^2a^2+\mu^2r^2+\Lambda\right)\right]R(r) = 0. \tag{2.29}$$

where Λ is the separation constant. The solutions of the angular equation (2.28) are spheroidal harmonics $S_l^m(\cos\theta; c)$, with the oblateness parameter $c \equiv a\sqrt{\omega^2-\mu^2}$ [53]. If this parameter is close to zero, the angular equation reduces to the angular part of the Laplace's equation in spherical coordinates. Therefore, in this limit, spheroidal harmonics become the spherical harmonics, with the separation constant $\Lambda = l(l+1)$ constrained by $l > |m|$ [53].

2.3.2 Unstable bound states

Given the complexity of the Kerr geometry, it is not surprising that analytic solutions for the radial equation (2.29) do not exist [32]. Nevertheless, one can suppose boundary conditions on the radial function such that bound states are possible. The field must

be ingoing at the event horizon and exponentially decaying towards spatial infinity. Such boundary conditions exist and are widespread in the literature [32] [54] [55]. An important consequence is that imposing a pair of boundary conditions automatically leads to a discrete spectrum of complex frequencies ω [50].

One may have an accurate idea of the bound states without trying to solve the radial equation with additional assumptions. Let us consider a new radial function

$$\psi(r) \equiv \Delta^{1/2} R(r). \tag{2.30}$$

Then, the radial equation (2.29) can be rewritten in the form of a Schrödinger-like equation

$$\frac{d^2\psi}{dr^2} + \left(\omega^2 - V_{eff}\right)\psi = 0, \tag{2.31}$$

where the effective potential is given by [54]

$$\begin{aligned} V_{eff}(r) = \omega^2 &- \frac{\omega^2\left(r^2+a^2\right)^2 - 4Mam\omega r + m^2a^2}{\Delta^2} \\ &- \frac{\Delta\left(\omega^2a^2 + \mu^2r^2 + \Lambda\right) + M^2 - a^2}{\Delta^2}. \end{aligned} \tag{2.32}$$

The asymptotic behavior of the effective potential at spatial infinity is given by [54]

$$V_{eff}(r) = \mu^2 - \frac{4M\omega^2 - 2M\mu^2}{r} + \mathcal{O}\left(\frac{1}{r^2}\right), \tag{2.33}$$

We will now simplify our ansatz for the field (2.8) and neglect the imaginary part of the complex frequency ω. The latter as well as the effective potential thus become real quantities. This simplification is motivated by the fact that the effective potential is complex, which makes the analysis of bound states more delicate. A track would be to split the Schrödinger-like equation into two equations for the real part and the imaginary part, and circumscribe some constraints on the bound states. Further investigations are required.

Our problem (2.31) is now completely analoguous to a quantum particle moving in a potential well V_{eff}. Consequently, bound states can be seen as frequency modes trapped in a potential well. If the asymptotic derivative of the effective potential is positive null, i.e. $dV_{eff}/dr = 0^+$, we have a trapping well [54]. By deriving the relation (2.33) and taking the limit at spatial infinity, a trapping well is hence possible if

$$\omega^2 > \frac{\mu^2}{2}. \tag{2.34}$$

This is the strict condition for having a trapping well. From (2.33), bound states are confined by the effective potential at spatial infinity if

$$\omega^2 < \lim_{r\to+\infty} V_{eff}\left(r\right) = \mu^2. \tag{2.35}$$

If we combine the equations (2.34) and (2.35), we find that bound states exist for modes

in the regime

$$\frac{\mu^2}{2} < \omega^2 < \mu^2. \tag{2.36}$$

One thus infers that the mass of the field traps the modes in the potential well, and prevents them from escaping to infinity. In summary, wave packets in this regime are bound to the black hole, in the sense that they orbit the black hole. In the literature, their orbits are said to be keplerian, in comparison with the two-body problem.

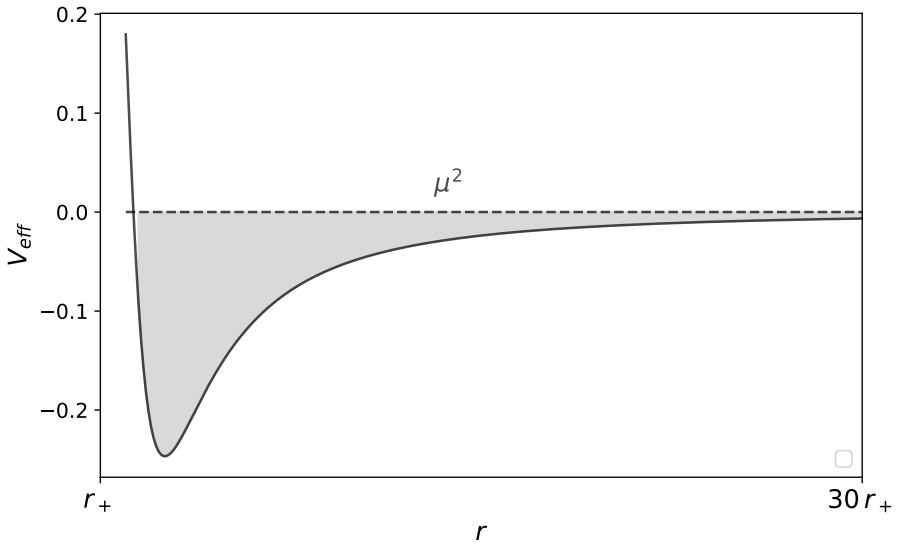

Figure 2.2: Plot of a potential well outside of a black hole ($r > r_+$) in the regime (2.36). Bound states are located in the trapping well (in gray) and confined by the nonvanishing potential at infinity μ^2 (dotted line).

In addition to the requirement (2.36) for the existence of a trapping well, one may look for bound states that are amplified via the superradiance process. Such unstable bound states, also called quasi-bound states, are possible if a trapping potential exists, and if the superradiance process takes place. One, therefore, realizes that these two conditions (2.25) and (2.36) are both satisfied in the regime

$$\frac{\sqrt{2}}{2}\mu < \omega < m\Omega_H. \tag{2.37}$$

Massive scalar waves in this regime grow with time while being confined by the trapping well. One could imagine that after a sufficiently long time-scale, a scalar field in this regime will populate the surrounding of the black hole, and form a scalar cloud. Its formation is facilitated if the mass of the field is sufficiently high to confine a maximal number of modes and if the event horizon rotates fast so that more trapped modes can grow in time. We are now ready to discuss the characteristic energy spectrum of a scalar cloud made of ultra-light bosons.

3 | Gravitational atom

Now that we know how to get an unstable scalar field, it is natural to wonder how the field populates the surroundings of the black hole, and at the same time forms a scalar cloud. As we will see, the peculiarity of this cloud is its hydrogenic energy levels. But before discussing its energy spectrum, let us introduce an important parameter involved in the dynamics of the scalar cloud. This parameter is called the gravitational fine-structure constant, and couples the mass of the black hole and the mass of the scalar field,

$$\alpha \equiv M\mu = \frac{r_g}{\lambda_c}, \tag{3.1}$$

where $r_g \equiv M$ is the gravitational radius of the black hole, and $\lambda_c \equiv \mu^{-1}$ is the reduced Compton wavelength of the field. The coupling constant α is hence equivalent to the ratio of the gravitational radius of the black hole, to the reduced Compton wavelength of the field. Note that r_g is nearly equal to $r_+ = M + \sqrt{M^2 - a^2}$, the size of the event horizon. In the following, we will thus juggle with r_g and r_+ without making distinctions. One can then estimate the order of the fine structure constant,

$$\alpha \simeq 0.01 \left(\frac{M}{M_\odot}\right) \left(\frac{\mu}{10^{-12}\mu_e}\right), \tag{3.2}$$

where $M_\odot$ is a solar-mass, and μ_e is the electron mass.

In 1979, through its pioneering article, Detweiler estimated the growth rate of a massive scalar field in the regime $\alpha \ll 1$, for which the growth rate can become important [32]. In particular, ultra-light bosons are affected by this regime, whatever the mass of the black hole. Some candidates are thus astrophysical black holes, as well as primordial black holes. The latter are particular since the Hawking radiation directly affects their fates, because of their weak mass compared to stars. In the following, we will assume the regime $\alpha \ll 1$ to hold, and we will see that it leads to hydrogen-like solutions for the scalar cloud.

3.1 Hydrogen-like solution

The equation of motion of a massive scalar field Φ can be approximated by the Schrödringer-like equation of an electron in the hydrogen atom. To achieve this goal, it is useful to

split the field into a particle and antiparticle contribution

$$\Phi(t,\mathbf{r}) = \frac{1}{\sqrt{2\mu}}\left[\psi(t,\mathbf{r})e^{-i\mu t} + \psi^*(t,\mathbf{r})e^{+i\mu t}\right], \tag{3.3}$$

where ψ is a complex scalar field, and ψ^* is its complex conjugate. One can arbitrarily turn off the second term of (3.3) and only consider the particle contribution in our discussion. Far from the gravitational radius $r \gg r_g$, the equation of motion of a complex massive scalar field is approximated by the Schrödinger equation for the hydrogen atom. Injecting the ansatz (3.3) into the wave equation (2.7), yields

$$i\frac{\partial}{\partial t}\psi(t,\mathbf{r}) = \left(-\frac{1}{2\mu}\nabla^2 - \frac{\alpha}{r}\right)\psi(t,\mathbf{r}), \tag{3.4}$$

where we keep only terms of order $\mathcal{O}(r^{-1})$ and $\mathcal{O}(\alpha)$, and ∇^2 is the Laplacian operator. Bound state solutions of the hydrogen atom are obtained by imposing the regularity of the wavefunction at the origin, and an exponentially decaying wavefunction at spatial infinity. These boundary conditions lead to the quantization of the energy. In our framework, since the Schrödinger equation (3.4) is valid far away from the gravitational radius, the boundary condition at the event horizon is replaced by a boundary condition at the origin in the electromagnetic case. Therefore, our problem is equivalent to an electron in the hydrogen atom, and solutions of (3.4) are automatically hydrogen-like.

3.1.1 Eigenfunctions

Combining the separability of the field in the Kerr spacetime (2.8) and our previous ansatz (3.3), gives a field ψ of the form

$$\psi(t,r,\theta,\phi) = e^{-i(\omega-\mu)t}\bar{R}(r)S(\theta,\phi), \tag{3.5}$$

where the original angular and radial functions in (2.8) are now replaced by

$$S(\theta,\phi) \equiv S(\theta)e^{im\phi}, \quad \text{and} \quad \bar{R}(r) \equiv R(r)\sqrt{2\mu}. \tag{3.6}$$

One then injects this new ansatz (3.3) into the Schrödinger equation (3.4) and gets a time-independent Schrödinger equation in order to get an eigenvalue problem

$$(\omega-\mu)\,\bar{R}(r)S(\theta,\phi) = \left(-\frac{1}{2\mu}\nabla^2 - \frac{\alpha}{r}\right)\,\bar{R}(r)S(\theta,\phi) \tag{3.7}$$

This is the typical eigenvalue problem of the hydrogen atom. Hence, eigenfunctions around the black hole are hydrogen-like and are indexed by three integers $\{n\ell m\}$. They respectively correspond to the principal, orbital, and magnetic "quantum numbers", which satisfy $\ell < n$ and $|m| \leq \ell$. An eigenfunction of (3.7) is thus

$$\psi_{n\ell m}(r,\theta,\phi) = \bar{R}_{n\ell}(r)Y_{\ell m}(\theta,\phi), \tag{3.8}$$

where $Y_{\ell m}(\theta, \phi)$ are spherical harmonics and $R_{n\ell}(r)$ are the hydrogenic radial functions. The radial functions are of the form [32]

$$\bar{R}_{n\ell}(r) = \sqrt{\left(\frac{2\mu\alpha}{n}\right)^3 \frac{(n-\ell-1)!}{2n(n+\ell)!}} \left(\frac{2\mu\alpha r}{n}\right)^{\ell} \exp\left(-\frac{\mu\alpha r}{n}\right) L^{2\ell+1}_{n-\ell-1}\left(\frac{2\mu\alpha r}{n}\right), \tag{3.9}$$

with $L^{2l+1}_{n-\ell-1}(x)$ the generalized Laguerre polynomial, which is defined by [53]

$$L^{2\ell+1}_{n-\ell-1}(x) = \frac{x^{-2\ell-1}e^x}{(n-\ell-1)!} \frac{d^n}{dx^{n-\ell-1}} \left(e^{-x}x^{n+\ell}\right). \tag{3.10}$$

Similarly to the case of an electron around a proton, estimating the average size of the scalar cloud is possible by using the expectation value of the radial coordinate,

$$r_c = \frac{r_g}{\alpha^2}\left(3n^2 - \ell(\ell+1)\right), \tag{3.11}$$

which can be approximated by $r_c \sim \frac{n^2}{\alpha^2} r_g$ for $l = m$ [56]. Consequently, for tiny couplings $\alpha \ll 1$, the cloud extends well beyond the event horizon, where a flat-spacetime approximation is justified since the Kerr spacetime is asymptotically flat. The scalar field is thus principally localized where spacetime is nearly flat. To avoid further confusions, let us clarify the following. In the rest of this thesis, we will use quantum terminology to describe the scalar cloud. In general, this appears to be appropriate since the size of the cloud is comparable to the Compton wavelength of ultra-light scalar particles. On the other hand, we will see that occupation numbers for all dynamically relevant levels are exponentially large in what follows so that all the dynamics can be accurately described by a classical field theory. For convenience, we will hence denote the eigenfunctions by $\psi_{nlm} \equiv |n\ell m\rangle$, refer to them as "states" and the eigenfrequencies as "levels".

3.1.2 Occupation density

Although we are working with a classical scalar field, one can define an occupation number for each state $|n\ell m\rangle$. Indeed, our action (2.4) for a scalar field is invariant under the transformation $\psi \to \psi\, e^{i\sigma}$, where $\sigma \in \mathbb{R}$ is a constant. The associated Noether current is thus

$$J^\nu = \frac{i}{2\mu}\left[\psi\nabla^\nu\psi^* - \psi^*\nabla^\nu\psi\right] - g^{0\nu}\psi^*\psi. \tag{3.12}$$

If we only keep terms of the order of r^{-1} in (3.12), the current density is roughly $J^0 \simeq \psi^*\psi$ [34]. We also know from (3.11) that the scalar cloud is principally located far away from the event horizon where spacetime is nearly flat. One can then interpret this current density as an occupation number density. The associated Noether charge of the scalar field ψ is approximately

$$N = \int d^3x\, \psi\psi^*, \tag{3.13}$$

which can be interpreted as an occupation number. Each state is now populated by a number of particles N_{nlm}.

Each state can be populated by an infinite number of particles since bosons are not affected by the Pauli exclusion principle. We would thus expect a normalisation constant

in the eingenfunctions (3.8) to take into account this bosonic behavior. Injecting an eigenfunction (3.8) into the integral for the occupation number (3.13) yields

$$N_{nlm} = \beta^2 \int d^3x \, \psi_{nlm}\psi^*_{nlm}, \tag{3.14}$$

where β is a normalisation constant. Since the hydrogen-like wavefunctions are normalized to one, one can further simplify this integral and get the normalisation constant $\beta = \sqrt{N_{nlm}}$. Finally, the general solution to the original scalar field Φ is a superposition of all eigenfunctions

$$\Phi(t, r, \theta, \phi) = \sum_{n,\ell,m} \sqrt{\frac{N_{nlm}}{2\mu}} e^{-i\omega_{n\ell m}t}\psi_{n\ell m}(r, \theta, \phi). \tag{3.15}$$

Some maps of the occupation number densities $|\psi_{n\ell m}|$ are shown in the Figure 3.1.

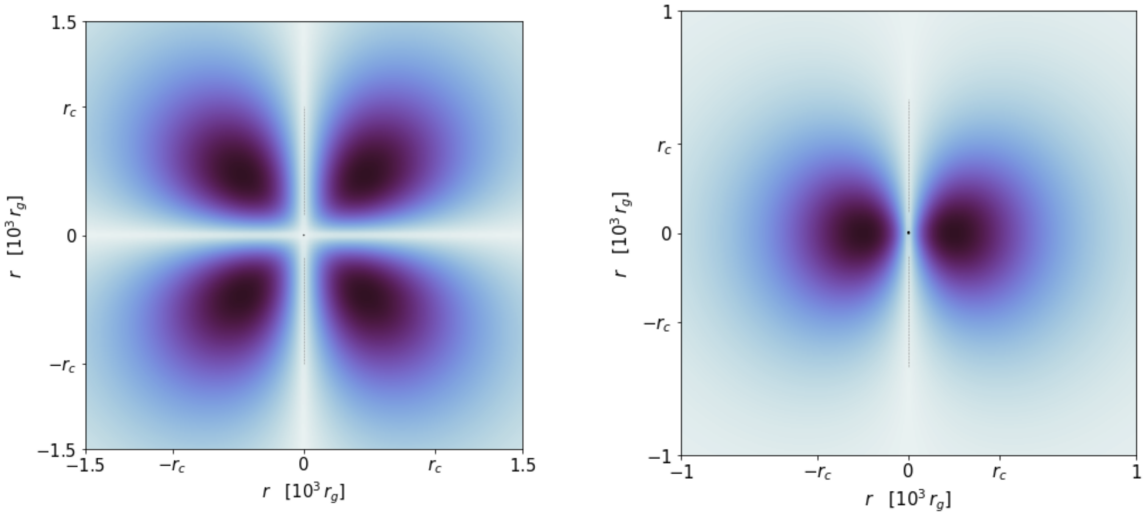

Figure 3.1: Occupation number density of the states $|321\rangle$ (on the left) and $|211\rangle$ (on the right) in the spin-axis plane of the black hole in Kerr-Schild coordinates, for $\alpha \approx 0.1$ and $M = 10\,M_\odot$. Darker regions correspond to higher density regions, and the dotted lines represent the spin axis. Each state peaks and extends well beyond the event horizon.

3.1.3 Eigenspectrum

The eigenfrequency spectrum is also hydrogen-like. One should note that some numerical results suggest that all the superradiant states are well approximated by a hydrogen-like spectrum, whatever the value of the coupling constant and the distance with respect to the event horizon [50]. In our case, the hydrogen-like spectrum naturally arises from the eigenvalue problem (3.7). It is given by

$$\omega_{n\ell m} = \mu\left(1 - \frac{\alpha^2}{2n^2}\right). \tag{3.16}$$

Note that keeping higher powers of r^{-1} in the equation of motion provide higher-order corrections to the eigenfrequencies, [57]

$$\Delta\omega_{n\ell m} = \mu\left(-\frac{\alpha^4}{8n^4} + \frac{(2\ell-3n+1)\alpha^4}{n^4(\ell+1/2)} + \frac{2\tilde{a}m\alpha^5}{n^3\ell(\ell+1/2)(\ell+1)}\right) \tag{3.17}$$

The corrections in (3.17) are analoguous respectively to the relativistic correction to the kinetic energy, the fine splitting ($l \neq 0$), and the hyperfine splitting ($m \neq 0$) of the hydrogen atom. In the following, we will solely conserve the lowest order (3.16).

In summary, far from the event horizon, a spinless boson cloud can bind to a black hole and occupies its surroundings as an electron around a proton. The energy spectrum of the scalar cloud is discrete and hydrogen-like. For these reasons, this hypothetical astrophysical system is called a gravitational atom. However, an obvious distinction between a hydrogen atom and the gravitational atom is of course the intrinsic nature of the coupling, which is gravitational and not electromagnetic. Moreover, electrons in the hydrogen atom are fermions, while the cloud is bosonic. This means that each discrete level of the gravitational atom could form a scalar cloud.

3.2 Growing or not growing

One may notice that the boundary conditions of our field are not exactly equivalent to the ones of the wavefunction in the hydrogen atom. Indeed, the field must be ingoing at the event horizon while the wavefunction must be regular at $r = 0$. For this reason, the inner boundary condition at the event horizon "forces" the eigenfrequency to be complex. Each state $|n\ell m\rangle$ is no longer stationary and now carries the complex eigenfrequencies

$$\omega_{nlm} \to \omega_{n\ell m} + i\gamma_{n\ell m}, \tag{3.18}$$

where the instability rate $\gamma_{n\ell m}$ was omitted in (3.16). We recall that the scalar field around a Kerr black hole (2.8) is decaying with time if $\gamma_{n\ell m} < 0$, or growing with time if $\gamma_{n\ell m} > 0$.

In general, the instability rate has to be computed numerically for any coupling constants α. However, as mentioned earlier, it can be obtained analytically for $\alpha \ll 1$. In this regime, this rate is given by [32]

$$\gamma_{n\ell m} = \frac{2r_+}{M} C_{n\ell m}\left(m\Omega_{\rm H} - \omega_{nlm}\right)\alpha^{4\ell+5}, \tag{3.19}$$

where

$$C_{nlm} \equiv \frac{2^{4\ell+1}(n+\ell)!}{n^{2\ell+4}(n-\ell-1)!}\left[\frac{\ell!}{(2\ell)!(2\ell+1)!}\right]^2 \prod_{j=1}^{\ell}\left(j^2\left(1-\frac{a^2}{M^2}\right) + 4r_+^2\left(m\Omega_H - \mu\right)^2\right). \tag{3.20}$$

One may remark that the sign of the instability rate (3.19) exclusively depends on the sign of $(m\Omega_H - \omega_{nlm})$. This implies that the instability rate for states in the superradiant regime, i.e. $\omega_{nlm} < m\Omega_H$, is always positive. Such states are called superradiant states and grow with time by extracting rotational energy from the black hole. On the other hand, states for which $m \leqslant 0$ always decay with time. Let us consider superradiant states

with $m > \omega_{n\ell m}/\Omega_H$

The superradiant rate is extremely sensitive to l, and it decreases when l increases [32]. Therefore, the fastest superradiant level carries the smallest possible l, i.e. the dipolar modes $l = m$. They are said to be dipolar since their moduli always take the form of two lobes. Unless otherwise specified, we will always consider dipolar modes. The fastest-growing states are hence of the form $|n11\rangle$, with $n > 1$. In general, for m and ℓ fixed, the fastest-growing rate occurs for the minimal value of n, i.e. $n = 2$ since $\ell = m = 1$. The state $|211\rangle$, which is the analog of the $2p$ state of the hydrogen atom, is thus the fastest-growing state of the scalar cloud. At the end of the superradiant growth of a given superradiant state $|n\ell m\rangle$, i.e. once the black hole's spin is not sufficiently high to satisfy the superradiance condition (2.25), higher energy levels with equal m will start to decay.

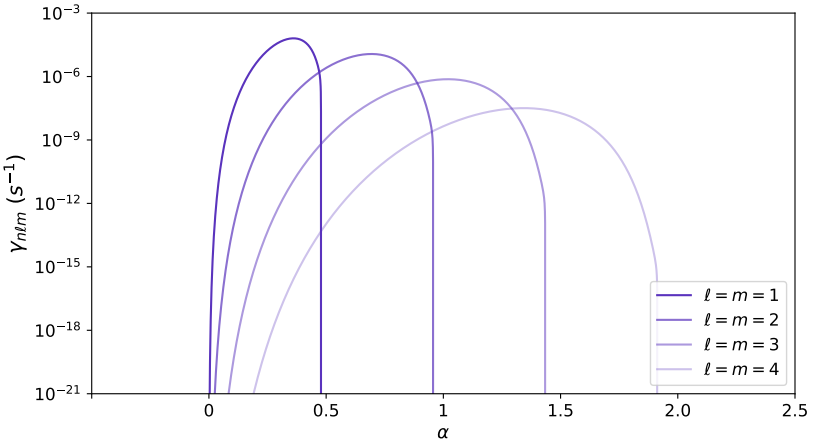

Figure 3.2: Superradiance rates of different dipolar modes $l = m$ with $n = 5$, for a $M = 10M_\odot$ and a = 0.9M. Note that here α is not necessarily smaller than one since the instability rate (3.19) remains valid if $\alpha/l \ll 1$ [33]. The superradiance condition requires that $\alpha/l \leq 1/2$. When α/l approaches its upper limit, the superradiant rate quickly drops and becomes negative for $\alpha/l > 1/2$. The superradiant rate peaks for a given value of α, which can be numerically computed.

Previously, we have seen that our hydrogen-like solution for the field (3.15) is expressed as a sum over every possible state. Identifying the occupation number of each superradiant state leads to the expected superradiant growth,

$$\frac{d}{dt}N_{n\ell m} \simeq \gamma_{n\ell m}\, N_{n\ell m}, \tag{3.21}$$

where $\gamma_{n\ell m}$ is the previous instability rate (3.19). The number of particles in a given superradiant state thus exponentially grows with time. Now that we have an idea of the dynamics of the scalar cloud, a legitimate track would be to detect them via certain signatures. In particular, one could think that these particles make transitions between different levels, like electrons in (hydrogen) atoms. However, given the nature of the coupling between the scalar particles and the black hole, the particularity of these transitions is that they would not be accompanied by an emission of photons, but by gravitons. The final chapter is devoted to the search for this specific signature.

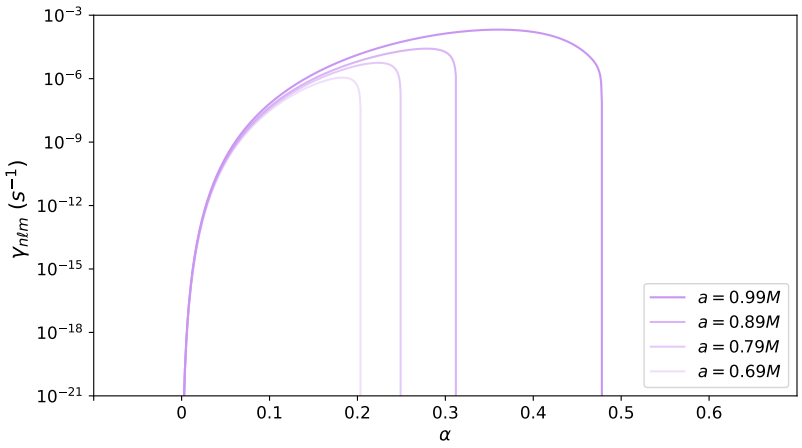

Figure 3.3: Superradiance rates of the state $|211\rangle$ and different values of the spin-to-mass ratio a, constrained by $a < M$ for a ten solar-mass black hole. Higher spins translate into higher instability rates.

4 | Continuous gravitational waves

4.1 Preliminaries

4.1.1 Plane harmonic waves

A formal study of the emission of gravitational waves from the cloud requires a rigorous and tedious treatment. In principle, we should linearize Einstein's equations assuming a background spacetime curved by the Kerr black hole and the backreaction of the cloud. Nevertheless, we can greatly simplify the task by making use of relevant assumptions. We know that the Kerr spacetime is asymptotically flat and that the cloud is mainly located far from the black hole horizon (cf. equation (3.11)). It is then natural to consider a simple Minkowski background to linearize the Einstein equations.

Formally, spacetime is decomposed into the Minkowski spacetime plus a small spacetime perturbation

$$g_{\mu\nu} = \eta_{\mu\nu} + h_{\mu\nu}, \tag{4.1}$$

with $|h_{\mu\nu}| \ll 1$. This is the weak field limit, which is valid at first order. Linearizing Einstein equations (9) is cumbersome but rather straightforward. The idea is to keep first ordrer terms in $h_{\mu\nu}$ for the Christoffel symbols, the Ricci tensor and the Ricci scalar. At the end of the process, the linearized form of Einstein equations yields a gravitational wave equation coupled to matter

$$\Box\bar{h}_{\mu\nu} = -16\pi T_{\mu\nu}, \tag{4.2}$$

where $T_{\mu\nu}$ is the energy-momentum tensor of the sources, and we define for convenience the "trace-reversed" perturbation $\bar{h}_{\mu\nu} \equiv h_{\mu\nu} - \frac{1}{2}\eta_{\mu\nu}\eta^{\alpha\beta}h_{\alpha\beta}$.
One can thus interpret gravitational waves as tiny perturbations of the background spacetime. The d'Alembert operator $\Box \equiv \eta^{\mu\nu}\partial_\mu\partial_\nu$ implies that gravitational waves travel at the speed of light, like electromagnetic waves. For completeness, note that the wave equation (4.8) is valid in the Hilbert gauge $\partial^\mu\bar{h}_{\mu\nu} = 0$.

An observer on Earth is far away from the Kerr black hole and its scalar cloud. It means that the observer is located in regions where the gravitational field of the source is negligible. Then, it is appropriate to use the linearised vacuum equation without sources

$$\Box\bar{h}_{\mu\nu} = 0, \quad \partial^\mu\bar{h}_{\mu\nu} = 0. \tag{4.3}$$

where the second equation is the Hilbert gauge, similar to the Lorenz gauge in electrodynamics. The Hilbert gauge involves four conditions, that reduce the ten independent

components of the symmetric metric tensor to six. But our gauge is not completely fixed. One can choose a coordinate system so that the metric tensor admits null temporal components $\bar{h}^{0\mu} = 0$, the traceless condition $\eta^{ij}\bar{h}_{ij} = 0$ and the transverse condition $\partial^i \bar{h}_{ij} = 0$. All these eight conditions define the transverse-traceless gauge, called the TT gauge, which now restricts the metric tensor to two independant components. We assume this gauge, for which $\bar{h}_{\mu\nu} = h_{\mu\nu}$, to hold in the following.

In analogy to electrodynamics, the general solution of the vacuum wave equation (4.3) is a superposition of plane harmonic waves. In our case, any such plane harmonic wave is of the form

$$h_{\mu\nu}(x) = \mathrm{Re}\left\{A_{\mu\nu} e^{ik_\mu x^\mu}\right\}, \tag{4.4}$$

with a symmetric amplitude tensor $A_{\mu\nu}$ and a real wave vector $k^\mu = (\omega, \mathbf{k})$ and $\omega = |\mathbf{k}|$. Consider now a coordinate system far away from the sources with cartesian spatial axes. Assuming an arbitrary propagation direction $\mathbf{k}$ along the z-axis gives the plane harmonic wave solution

$$h_{ij}(t, z) = A_{ij} \cos[\omega(t - z)], \tag{4.5}$$

with the amplitude tensor

$$A_{ij} = \begin{pmatrix} h_+ & h_\times & 0 \\ h_\times & -h_+ & 0 \\ 0 & 0 & 0 \end{pmatrix}. \tag{4.6}$$

The h_+ and $h_\times$ are called the amplitudes of the "plus" and 'cross" polarisation of the gravitational waves. Their interpretation comes naturally if we express the line element of the general metric tensor (4.1) from the vacuum solution (4.5):

$$\begin{aligned} ds^2 = &- dt^2 + + \{1 + h_+ \cos[\omega(t - z)]\}\, dx^2 + 2h_\times \cos[\omega(t - z)] dx dy \\ &+ \{1 - h_+ \cos[\omega(t - z)]\}\, dy^2 + dz^2. \end{aligned} \tag{4.7}$$

We observe that the plus mode affects the proper distance in the x and y directions, separately, while the cross mode mixes them. Both modes produces a time-periodic elliptic deformation of pulsation ω in the planes perpendicular to the propagation direction $\mathbf{k}$ (or the z-axis). For the plus mode, the main axes of the ellipse coincide with the coordinate axes, while for the cross mode they are rotated by 45°. Therefore, if the coordinate system is rotated by 45°, the two modes interchange. This is in analogy with electromagnetic waves, where there are waves linearly polarised in the x direction and waves linearly polarised in the y direction. Rotating the coordinate system by 90° automatically interchanges their roles.

4.1.2 Sources and waves

The production of gravitational waves depends on the properties of the sources. For this purpose, let us come back to the wave equation coupled with sources

$$\Box \bar{h}_{\mu\nu} = -16\pi T_{\mu\nu}. \tag{4.8}$$

The source term satisfies a conservation law. Indeed, differentiating (4.8) in the Hilbert gauge gives

$$\partial^\mu T_{\mu\nu} = 0. \tag{4.9}$$

This current conservation (4.9) implies that the energy of the source as well as its momentum are conserved. This is valid whatever the properties of sources, because this is a first order theory. In a non-linear theory of general relativity, the covariant divergence of the energy-momentum tensor vanishes instead.

The general solution of (4.8) is a combination of the plane harmonic waves plus a particular solution to the inhomogeneous equation. Such a particular solution can be obtained by analogy with the retarded potentials from electrodynamics

$$\bar{h}_{\mu\nu}(t,\mathbf{r}) = \frac{1}{4\pi}\int d^3x'\, 16\pi \frac{T^{\mu\nu}\left(t-|\mathbf{r}'-\mathbf{r}|\,,\mathbf{r}'\right)}{|\mathbf{r}'-\mathbf{r}|}, \tag{4.10}$$

where the primed coordinates correspond to the source's mass distribution. Since the cloud is localized in the black hole environment, we should consider the far-field approximation. The latter assumes that the dimension of the source is negligible with respect to the distance from it. Consequently, the particular solution is now approximated by

$$\bar{h}_{\mu\nu}(t,r) = \frac{4}{r}\int d^3x'\, T_{\mu\nu}\left(t-r,\mathbf{r}'\right). \tag{4.11}$$

The perturbative metric $h_{\mu\nu}$ exclusively depends on $\mathbf{r}$ in terms of its modulus r, which means that wave fronts are spheres. In any region where the far-field approximation is valid, the radii of these spheres are huge and the curvature is negligible. Gravitational waves are thus well approximated by plane waves.

One should remark that the component $\bar{h}_{00}$ is related to the Newtonian gravitational potential,

$$\bar{h}_{00}(t,r) = \frac{4}{r}\int d^3x'\, T_{00}\left(t-r,\mathbf{r}'\right) = \frac{4}{r}M, \tag{4.12}$$

where M is the mass (or energy) of the source. From the conserved current (4.9), the mass is conserved and the time-dependancy drops out. This reasoning is also valid for the components $\bar{h}_{0i}$, except that the momentum of the matter is now conserved. To get a more interesting picture of the problem, we should look at the spatial components of the metric,

$$\bar{h}_{ij}(t,r) = \frac{4}{r}\int d^3x'\, T_{ij}\left(t-r,\mathbf{r}'\right). \tag{4.13}$$

Even if this integral is not a conserved quantity, one can relate it to the properties of the source. We must introduce the mass multipole moment of the source.

In electrodynamics, an electric dipole generates electromagnetic waves. In general relativity, we will see that a mass quadrupole generates gravitational waves. This arises from the nature of the metric tensor, which is a rank-2 tensor, while the electromagnetic four-potential is a rank-1 tensor. The quadrupole moment of the source is defined by

$$Q^{ij}(t) = \int d^3x'\, T_{00}(t,\mathbf{r})x^i x^j, \tag{4.14}$$

where x^i is the k^{th} component of the four-position $x^\mu = (t,x,y,z)$, and T^{00} is the energy density of the source. Differentiating twice the quadrupole moment (4.14), using the Minkowskian conservation law of the stress-energy tensor (4.9), and relating the derivative

with the retarded solution (4.11) result in the wave tensor

$$\bar{h}^{ij}(t,r) = \frac{2}{r}\frac{d^2Q^{ij}}{dt^2}, \tag{4.15}$$

where the derivative is evaluated at the retarded time $t-r$. This formula translates the quadrupolar production of gravitational waves. One should note that the metric tensor involves the second time derivative of the mass quadrupole moment, while the electromagnetic 4-potential involves the first time derivative of the electric dipole moment. The wave tensor (4.17) can be projected on the TT gauge by making use of the following projector

$$P_{ij} \equiv \delta_{ij} - n_i n_j, \tag{4.16}$$

with $n_i = x^i/r$. Finally, we get

$$h^{k\ell}(t,r) = \frac{2}{r}\frac{d^2\mathbb{Q}^{k\ell}}{dt^2}, \tag{4.17}$$

with $\mathbb{Q}_{ij} \equiv P_{ik}Q^{kl}P_{lj} - \frac{1}{2}P_{ij}P_{kl}Q^{kl}$. The first term corresponds to the transverse part, while the second term correponds to the traceless part.

4.1.3 Quadrupolar radiation

In the previous section we have seen that gravitational waves are small perturbations of the immutable Minkowski background. One can then assign a quadrupolar radiation by the sources, also called the luminosity by astronomers

$$\frac{dE}{dt} = \frac{1}{5}\left\langle \frac{d^3\mathbb{Q}^{k\ell}}{dt^3}\frac{d^3\mathbb{Q}^{k\ell}}{dt^3} \right\rangle, \tag{4.18}$$

where the derivatives are also evaluated at the retarded time $t-r$ [58]. The brackets stand for the time average, which is defined over the typical timescale of the production. This luminosity is analoguous to the Larmor formula in electrodynamics, except that now one has third derivatives instead of second derivatives.

In principle, we could get the general quadrupolar radiation from the scalar cloud. We implicitely know the energy density of the scalar cloud, since we derived the energy-momentum tensor of a scalar field (2.10) and the gravitational atom solutions for the field (3.8). We should then insert this energy density into the integral of the quadrupole moment (4.14). Work has been done in this direction and result in a quadrupole moment for the cloud exclusively proportionnal to its mass and its squared size [34]. Nevertheless, we should derive it twice with respect to time. It requires some knowledge about the dynamic of each parameter involved in the superradiant rates (3.19). In particular, we still do not know how the cloud's evolution precisely affects the black hole's spin and the size of its event horizon. Further theoretical investigations are required.

It is now time to simplify the luminosity relation (4.18). For this purpose, the coordinate system is glued to the source and its z-axis is oriented towards the Earth. There are hence no distinctions between the distance from the source r and the z component. One can differentiate relation (4.17) and inject the result into the power radiated away (4.18).

This results in

$$\frac{dE}{dt} = \frac{r^2}{20}\left\langle \frac{dh^{k\ell}}{dt}\frac{dh^{k\ell}}{dt}\right\rangle. \tag{4.19}$$

Since an observer on Earth is far away from the source, we can also make use of the vacuum solutions (4.5) and further simplify the expression

$$\frac{dE}{dt} = \frac{\omega^2 r^2}{10}\left\langle h_+^2 \sin^2[\omega(t-r)] + h_\times^2 \sin^2[\omega(t-r)]\right\rangle. \tag{4.20}$$

The time average contains each polarization amplitude, with identical periods (or identical pulsations). Consequently, the time average only depends on the periodic term $\sin^2(\omega(t - r/c))$, for which the average value over a period is one half, and the power radiated away becomes

$$\frac{dE}{dt} = \frac{\omega^2 r^2}{20}h^2, \tag{4.21}$$

where we define a new strain amplitude $h \equiv \sqrt{h_+^2 + h_\times^2}$. For convenience, we will denote the power $P = dE/dt$ and rearrange the previous equation as follows

$$h = \sqrt{\frac{20P}{\omega^2 r^2}}. \tag{4.22}$$

Even if the power is still unknown, this a small progress since now the power does not explicitely depend on the polarisation of the source[1]. Now, it is natural to introduce a new framework to describe the power radiated during transitions.

4.2 Level transitions

4.2.1 Emission of gravitons

Analogously to atomic transitions emitting photons, level transitions of ultra-light scalar particles around black holes should emit gravitons. These are at the heart of quantum gravity theories. Many candidate theories exist, the most popular are certainly string theory and loop quantum gravity. Obviously, using these frameworks is out of scope since our discussion only cares about elementary aspects of quantum gravity. Moreover, we do not need to rely on the existence of gravitons to explain bosonic transitions: these can be also treated with gravitational waves. However, the quantum formalism is more intuitive in our context.

As we have seen in the last section, electrodynamics and gravity present many analoguous features. The quanta associated with the electromagnetic waves are photons. Similarly, the quanta associated with the gravitational waves are gravitons, which are now spin-2 particles because the metric tensor has two indices. More precisely, it comes from the invariance of the wave metric under a rotation of 180° in the plane $x - y$. A graviton is a quantum with a four-momentum

$$p^\mu = \hbar k^\mu, \tag{4.23}$$

[1]Note that there is a difference of $\sqrt{5}$ in equation (4.32) with respect to [56].

where k^μ is the original wave vector in the plane harmonic wave solution (4.5). One can thus interpret the gravitational radiation (4.18) by any sources as the emission rate of gravitons of energy ω

$$dP = \hbar\omega d\gamma_q, \tag{4.24}$$

where $d\gamma_q$ is the number of gravitons emitted per second for an infinitesimal power dP [59]. In our framework, we are concerned by bosonic transitions. The energy of gravitons corresponds to the energy difference between two hydrogen-like levels (3.16), which is

$$\hbar\omega = \frac{1}{2}\mu\alpha^2\left(\frac{1}{n_g^2} - \frac{1}{n_{\mathrm{e}}^2}\right), \tag{4.25}$$

where n_g and n_e are the principal quantum number respectively of a lower energy level and an excited energy level, such that $n_g < n_e$. More generally, integrating the equation (4.24) over the solid angles yields

$$\gamma_q = \frac{1}{\hbar\omega}\int d\Omega\, \frac{dP}{d\Omega}, \tag{4.26}$$

which can be used to compute the emission rate of gravitons. The missing ingredient is the power radiated per solid angle. An analytic solution exists and it is based on a Fourier expansion of the energy-momentum tensor [59]. Althought this method effectively leads to an expression of the power radiated per solid angle, the trade-off is to deal with many unusable terms in the expansion. In our discussion of bosonic transitions, it is sufficient to get the dependencies of the single term associated with the emission rate of gravitons during transitions, which is of the order of

$$\gamma_t \sim \frac{2\omega^5}{5}\mu^2 r_c^4 \tag{4.27}$$

with r_c the average radius of the cloud (3.11) [33]. It is completely negligible with respect to the superradiant rate (3.19) but it becomes relevant when many particles populates the levels.

4.2.2 Kinetic description

It is now time to describe the evolution of the occupation numbers and the resulting amplitude. We assume that two energy levels dominate the evolution of the cloud. In this way, the emitted gravitons are only due to transitions between two levels, an "excited" level and a "ground" one. The gravitons are thus monochromatic.
Each level increases its population via the superradiance process or ingoing transitions. On the other hand, the number of particles within a level decreases due to transitions. Let us consider the simplified kinematic equations for the excited level

$$\frac{dN_e(t)}{dt} = \gamma_e N_e - \gamma_t N_g N_e - \gamma_t N_e, \tag{4.28}$$

and the ground level

$$\frac{dN_g(t)}{dt} = \gamma_g N_g + \gamma_t N_g N_e + \gamma_t N_e, \tag{4.29}$$

where $\gamma_{g,e}$ are the superradiant rates of each level (3.19) [60]. The second term corresponds to stimulated emission caused by the self-gravitational interaction of the cloud, while the third term corresponds to spontaneous emission. The latter contribution has a tiny influence on the evolution of the cloud when many particles populates the ground level, i.e. when $\gamma_t N_g N_e \gg \gamma_t N_e$.

Since $\gamma_t \ll \gamma_{e,g}$, the transitions are negligible if the scalar cloud is small. Both levels grow exponentially with their respective superradiant rates. The transition term become relevant when they start to compete with the superradiant growth term. The occupation number of the excited level is maximized when its derivative vanishes, which occurs for

$$N_g = \frac{\gamma_e - \gamma_t}{\gamma_t}. \tag{4.30}$$

A single graviton is emitted during a bosonic transition. Intuitively, the number of graviton emitted per second is hence equal to the number of bosonic transitions per second. Consequently, from (4.24), the power radiated also depends on the transition rate

$$P = \omega\gamma_q = \omega\gamma_t N_e(N_g + 1), \tag{4.31}$$

and the strain amplitude (4.32) becomes

$$h(t) = \sqrt{\frac{20}{\omega r^2}\gamma_t N_e(t)(N_g(t) + 1)}, \tag{4.32}$$

This relation is particularly useful since now the evolution of the population explicitely dictates the amplitude. What about the maximal strain amplitude ?

Our following analysis is based on these initial conditions. Let us consider a stellar black hole of mass $M = 10M_\odot$ with a spin $a = 0.9M$. Such black hole mass provides the highest superradiant rates, and hence the highest growing timescale of the cloud. Since we are dealing with the regime $\alpha/\ell \ll 1$ and a 10 solar-mass black hole, the mass of the probed ultra-light scalars is below 10^{-10} eV. Obviously, we are looking for the maximal strain that occurs during the evolution of the cloud. From the relation (4.32) along with the kinetic relations (4.28) and (4.29), the strain is proportional to

$$h_{max} \propto \frac{\gamma_e}{\sqrt{\omega\gamma_t}}. \tag{4.33}$$

Consequently, one should maximize the superradiant rate of the excited level, and minimize the transition rate as well as the transition frequency. From the previous chapter, we already know how to maximize the superradiant rate. One should look for dipolar modes $\ell = m$, constrained by a rather small principal quantum number and the superradiance condition $m > \omega/\Omega_H$. Moreover, there is a unique peak value for each superradiant state (at fixed black hole mass and fixed spin), which means that a single bosonic mass μ maximizes the superradiant rate. On the other hand, minimizing both the transition rate (4.27) and the transition frequency requires close energy levels with a minimal principal quantum number. Therefore, the difference between each principal quantum number $n_e - n_g$ should be one. For convenience, we assume a unique couple (ℓ,m) for both excited and ground levels.

In summary, the most promising transitions, which maximize the peak strain, verify

$$|nll\rangle \to |n-1\, ll\rangle, \tag{4.34}$$

where n is sufficiently small.

4.2.3 Numerical study

Our current goal is to model the typical behavior of each occupation number and the emission amplitude. One would naively search for an analytic solution of the kinetic equations (4.28) and (4.29). Nevertheless, they constitue a set of inhomogeneous and coupled nonlinear differential equation of first order, where the nonlinear component is the stimulated emission. It is thus necessary to look for numerical solutions. For this purpose, we can rewrite the kinetic equations in a matrix form

$$\frac{d}{dt}\begin{pmatrix} N_g(t) \\ \\ N_e(t) \end{pmatrix} = \begin{pmatrix} \gamma_g + \gamma_t N_e(t) & \gamma_t \\ \\ -\gamma_t N_e(t) & \gamma_e - \gamma_t \end{pmatrix} . \begin{pmatrix} N_g(t) \\ \\ N_e(t) \end{pmatrix} \tag{4.35}$$

The solution to this set of differential equations must satisfies

$$\begin{pmatrix} N_g(t+\delta t) \\ \\ N_e(t+\delta t) \end{pmatrix} = \int_t^{t+\delta t} dt' \begin{pmatrix} \gamma_g + \gamma_t N_e(t') & \gamma_t \\ \\ -\gamma_t N_e(t') & \gamma_e - \gamma_t \end{pmatrix} . \begin{pmatrix} N_g(t) \\ \\ N_e(t) \end{pmatrix} + \begin{pmatrix} N_g(t) \\ \\ N_e(t) \end{pmatrix}, \tag{4.36}$$

where $\delta t \in \mathbb{R}^+$ must be negligible with respect to the timescale of the superradiant process $\delta t \ll \gamma_{e,g}^{-1}$. In this limit, the integral is similar to the surface of a riemannian rectangle and the solutions approach

$$\begin{pmatrix} N_g(t+\delta t) \\ \\ N_e(t+\delta t) \end{pmatrix} = \delta t \begin{pmatrix} \gamma_g + \gamma_t N_e(t) & \gamma_t \\ \\ -\gamma_t N_e(t) & \gamma_e - \gamma_t \end{pmatrix} . \begin{pmatrix} N_g(t) \\ \\ N_e(t) \end{pmatrix} + \begin{pmatrix} N_g(t) \\ \\ N_e(t) \end{pmatrix}, \tag{4.37}$$

for any values of t if δt is sufficiently small. Starting from an initial condition $N_g(t=0) = 1$ and $N_e(t=0) = 1$, this simple algorithm computes the solution at the first step $t_1 = \delta t$. Then, it uses this approximated solution as an initial condition for the second step $t_2 = t_1 + \delta t = 2\delta t$. Our numerical solution is thus computed by recurrence, with the simple relation $t_i = i\delta t$, with $i \in \mathbb{N}$.
To verify that the approximate solutions are realistic, we compare the value of the occupation number of the ground level for which the maximal occupation number of the excited level occurs and compare with the analytic solution (4.30).

4.2.4 Results

In this section, we present the evolution of the occupation numbers and how the strain is affected for dipolar modes $l = m$. Our system is a stellar black hole of mass $M = 10M_\odot$ at 10 kpc away with a spin-mass ratio $a = 0.9M$. Our initial condition is one particle per level at $t = 0$. We consider the bosonic transition $n_e = 6$ to $n_g = 5$, with $\ell \leq 4$, which

allows us to play with various l. Finally, we remind the reader that the weak coupling regime $\alpha/\ell \ll 1$ still holds, and we take $\alpha/l = 0.3$.

Minimal case: $\ell = m = 1$

This simulation is presented in Figure 4.1. The probed ultra-light scalar has a mass of $\mu = 4.\,10^{-12}$ eV. The superradiance rate of the ground level is $\gamma_g = 0.33$ days^{-1}, while the superradiance rate of the excited level $\gamma_e = 0.22$ days^{-1}.

Let us first discuss the physics behind the simulation. We are in the case where the superradiant rate of the excited level is lower than the superradiant rate of the ground level, i.e. $\gamma_e < \gamma_g$. It simply arises from the fact that the superradiance rate (3.19) is generally lower for higher n. We observe that the excited level depopulates very quickly once it reaches the maximum after nearly 500 days. The transition term for the ground state does not affect the evolution of the ground level. The evolution of the strain amplitude (4.32) depends on the transition term and follows the behavior of the excited level. A continuous gravitational-wave signal is thus emitted at a tiny peak strain $h_{max} \approx 10^{-29}$ and only lasts some days. Therefore, this minimal case may not be an appropriate observation channel.

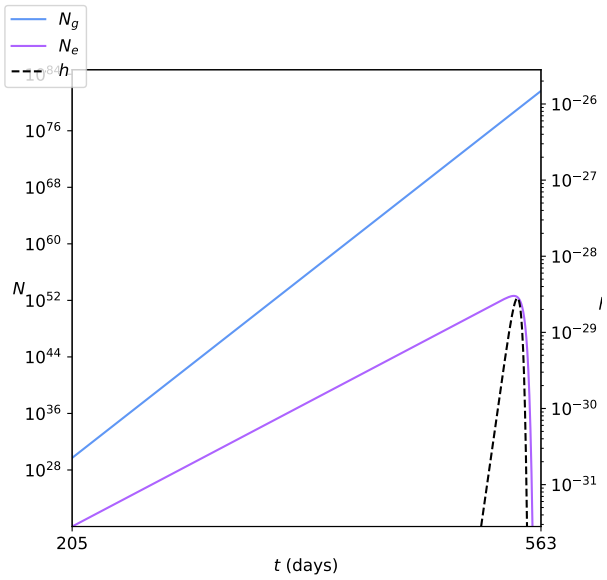

Figure 4.1: Evolution of the strain amplitude (right y-axis and black dashed curve) and the occupation numbers (left y-axis) of the ground level (in blue) and the excited level (in purple) for the bosonic transition $|611\rangle$ to $|511\rangle$. The frequency of the emitted gravitons is about 0.5 Hz.

Maximal case: $\ell = m = 4$

This simulation is presented in Figure 4.2. The probed ultra-light scalar particle has a mass of $\mu = 1.6\,10^{-11}$ eV. The superradiance rate of the ground level is $\gamma_g = 2.73\,10^{-4}$ years^{-1}, while the superradiance rate of the excited level $\gamma_e = 2.18\,10^{-4}$ years^{-1}.

We compare our results with a previous simulation by A. Arvanitaki et al. in 2015, with identical conditions [60]. Since $\gamma_e < \gamma_g$, the evolution is similar to the previous case.

However, one should observe some notable differences with the results of A.Arvanitaki et al.. First, our peak amplitude is 10^5 smaller in our case and happens after nearly 500 000 years. Second, our maximal occupation number of the excited level occurs at $N_g \approx 10^{67}$, while it happens at $N_g \approx 10^{70}$ for the other simulation. These discrepancies are due to the distinct computation methods of the superradiant rates. In this thesis, we have used the analytic result from Detweiler (3.19). The latter is rather practical since it directly relates the effects of each parameter on the superradiance rate. A. Arvanitaki et al. proceed differently. They have used a numerical approach, which is more appropriate, and the latter is also valid in the weak coupling regime $\alpha/\ell \ll 1$. These computation methods are equivalent at tiny couplings $\alpha/l \ll 1$ and small ℓ, but they quickly start to diverge when l increases (cf. Figure 4.3 for a detailed comparison between each method). Their method is thus more convenient for the maximal case. Concerning the strain, a continuous gravitational-wave signal is emitted at a peak strain $h_{max} \approx 5.\,10^{-26}$ and lasts some decades. Therefore, this maximal case should be a more appropriate observation channel.

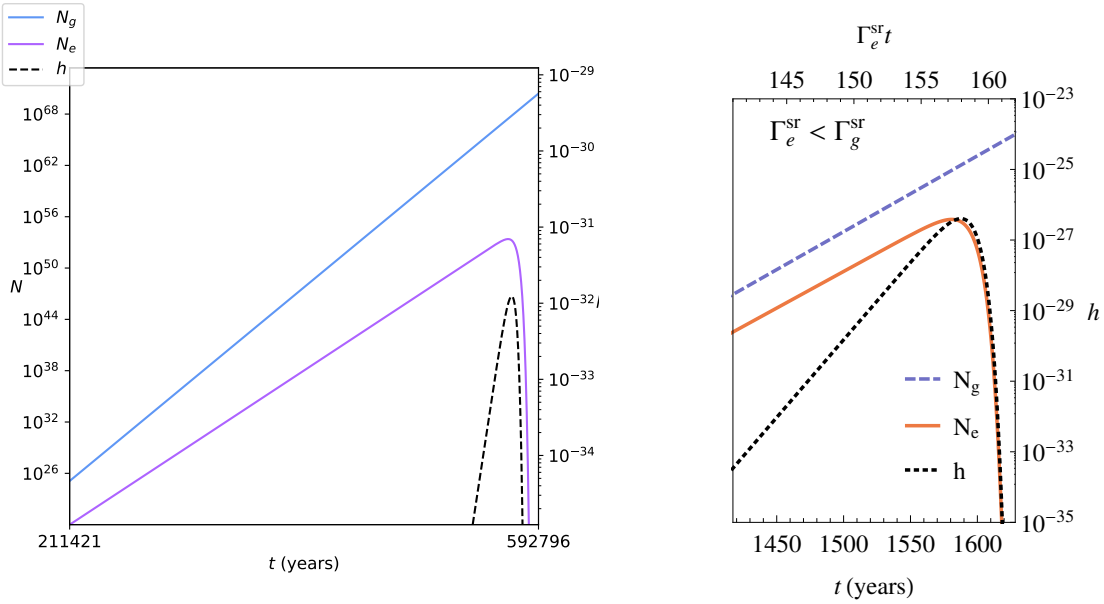

Figure 4.2: Evolution of the strain amplitude (right y-axis and black dashed curve) and the occupation numbers (left y-axis) of the ground level (in blue) and the excited level (in purple or orange) for the bosonic transition $|644\rangle$ to $|544\rangle$. The Figure on the left corresponds to our simulation, while the Figure on the right is the previous one by A. Arvanitaki et al. in 2015 [60]. The frequency of the emitted gravitons is about 38 Hz.

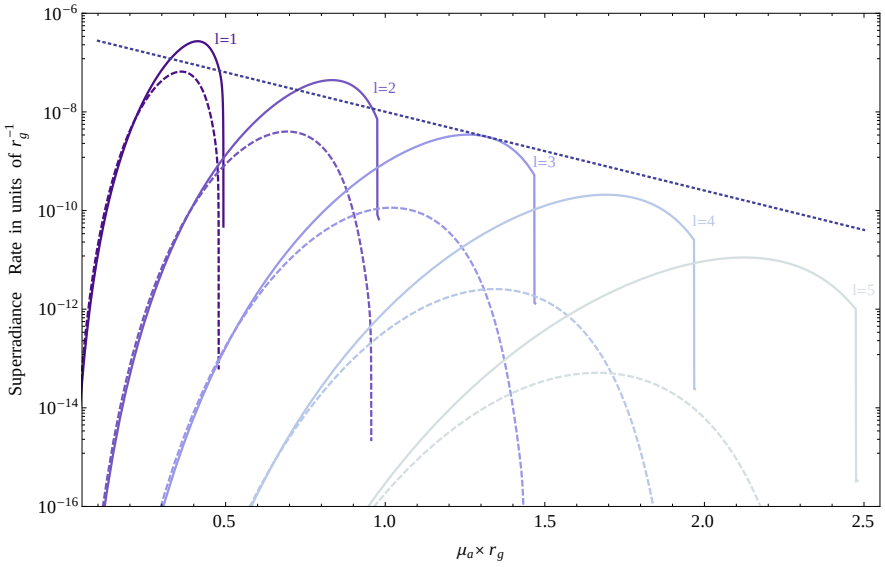

Figure 4.3: From [33]. Superradiance rates obtained with the Detweiler method (solid lines) and the semi-analytic method (dashed lines) for a near extremal black hole $a = 0.99\,M$ and a constant principal quantum number ℓ. Each color corresponds to a superradiant state with a given angular quantum number $\ell = m$. Both methods are indeed equivalent at tiny couplings $\alpha/l \ll 1$, but they quickly start to diverge when l increases. The difference between each method is more pronounced at high orbital quantum number ℓ. Our superradiance rates for the maximal case $l = m = 4$ are at least smaller for any value of α, which translate into the listed discrepancies in Figure 4.2. On the other hand, the superradiance rates for the minimal case $l = m = 1$ are similar for both methods.

Conclusion

This journey to the heart of scalar clouds around spinning black holes ends here. We have explicitly described the main steps in the formation of such clouds. The first ingredient is a spinning black hole. Since these are the result of the gravitational collapse of massive stars, this class of black holes is ubiquitous in our Universe. The second ingredient is a process to extract rotational energy from these "cosmic spinning tops". First, there is the Penrose process which requires sending a massive particle, or a macroscopic object, towards the black hole through an appropriate geodesic. More generally, superradiance is the analogous process and works by sending a wave packet to the event horizon with an appropriate angular frequency. Finally, the third ingredient is to confine this energy extracted from the reflected wave packet. We have identified the conditions to have a confined and superradiant scalar field.

With these three ingredients, we were able to describe the energy levels of an ultra-light scalar field coupled with an astrophysical black hole. The classically treated field has then taken on quantum properties. The field behaves like a gravitational atom with hydrogen-like energy levels and hydrogen-like state occupation. Nevertheless, since this field is bosonic, the states can be occupied by an infinite number of particles and grow via the superradiance process until the mode is completely extracted. The gravitational atom then becomes a cloud made of scalar particles. Intuitively, similarly to the photon emission during electronic transitions in "classical" atoms, we were interested in the graviton emission during bosonic transitions in the cloud.

Concerning the energy levels and the superradiance growth rates, we have exclusively worked in the weak regime $\alpha/\ell \ll 1$. However, we can still draw some conclusions from the simulations. By looking at the different $\ell = m$ dipole modes, we have deduced that maximizing the orbital quantum number leads to the most promising gravitational signals. Nevertheless, it would be interesting to perform a similar analysis for stellar or supermassive black holes in the regime $\alpha/\ell \approx 1$. In this way, we could compare our simulations and refine our estimate of the peak amplitude and its duration. Along with these considerations, let us also note that this work also aims to concisely synthesize the topic.

The initial problem concerns clouds composed of scalar bosons. Nevertheless, we should also extend to vector bosons since these are also dark matter candidates. They are affected by superradiance and should also form unstable bound states around black holes. The popularity of this study suffers from its more complex formalism than scalar bosons. Let us also mention that an interesting track would be to consider Kerr-Newmann black holes and to study how charged particles are affected via the superradiance, which in this case will also depend on the respective charges of the black hole and the particles.

Some effects have been neglected in the work. First of all the accretion of matter by

the black hole. If scalar particles exist, they should be accreted by the black hole and contribute to the formation of the cloud. The kinetic description of our levels thus lacks an accretion term. Second, the back-reaction of the cloud and the accretion disk on the Kerr metric has also been neglected throughout the calculations. Third, we only consider two levels in our simulations. A more global description would be welcome. Then, let us also mention the annihilation process of dark matter particles. This process should be preponderant in the evolution of the cloud and lead to the emission of gravitons. Ideally, the effective cross-section of such a process should be calculated, although the annihilation rate can be estimated via the Fourier series expansion of the field energy-momentum tensor. Finally, note that we have treated a free scalar field, but gravitational interactions between the particles should be felt when the bosonic cloud is huge and lead to the sudden collapse of the cloud into a bosenova [56]. There is still a lot of work to do.

What about the future? As we have seen, bosonic transitions occur at small frequencies, typically below 50 Hz, while our current interferometers principally work above 20 Hz. In the future, many upcoming detectors should be designed in this frequency domain and hence increase our chance to observe these bosonic transitions. Figure 4.4 shows the sensitivities of next-generation detectors.

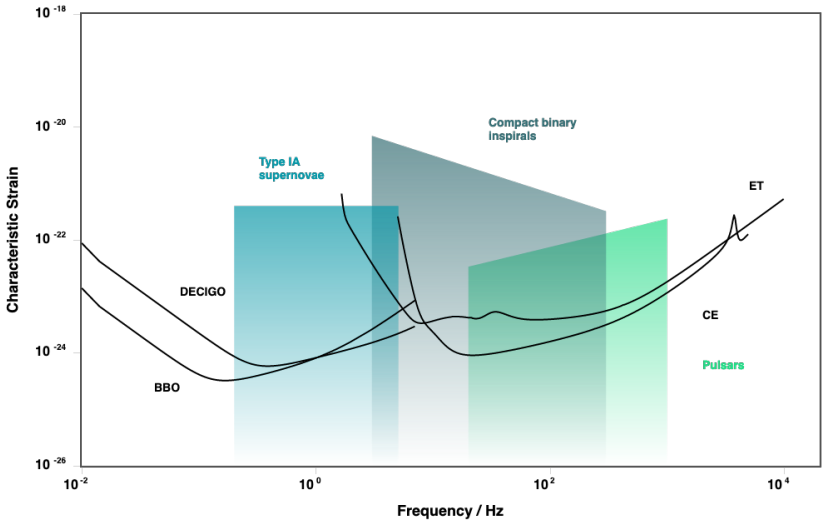

Figure 4.4: From the website `www.gwplotter.com`. Comparison of the characteristic detector sensitivity as a function of gravitational wave frequency for next-generation detectors, which should work in the appropriate frequency domain of bosononic transitions. The typical strain amplitude of astrophysical sources are also presented. There are two space-based projects, with the Deci-hertz Interferometer Gravitational wave Observatory (DECIGO) and the Big-Bang Observer (BBO), and two ground-based projects, with the Cosmic Explorer (CE) and the Einstein Telescope (ET).

To conclude, a promising prospect would be to calculate the evolution of the quadrupole moment of the cloud during the orbital motion. However, it would be necessary to model the accretion of a Kerr black hole as well as the deformation of the event horizon by the cloud itself. Thus, it would be possible to precisely capture the power radiated in the form of gravitational waves for each polarization. This scenario is not yet written, but the GW150914 event should serve as a muse...

A | Killing vector

Killing vectors are widespread tools in General Relativity. They are used to classify the *continuous* symmetries of a metric. To illustrate what is a Killing vector, a convenient toy model is the 2-sphere. This is simply the locus in $\mathbb{R}^3$ at a unit distance from the origin. The line element between two close points on the sphere is given by

$$ds^2 = \sin^2\theta\, d\phi^2 + d\theta^2. \tag{A.1}$$

Now, imagine that we apply an infinitesimal rotation onto a point of the sphere about the z-axis

$$\phi \to \phi + d\phi, \tag{A.2}$$

where $d\phi$ is an infinitesimal scalar. A rotation about the z-axis means a translation of this point in the ϕ direction. The infinitesimal displacement vector in this direction is thus simply

$$\mathbf{k} = (d\phi, 0), \tag{A.3}$$

since we are working in the polar coordinates (ϕ, θ). The metric (A.1) is clearly invariant under a rotation about the z-axis simply because it does not depend on the coordinate ϕ. The displacement vector $\mathbf{k}$ thus preserves the metric and is called a Killing vector. It is usually noted

$$\mathbf{k} \equiv \mathbf{k}/d\phi = (1, 0), \tag{A.4}$$

or equivalently

$$\mathbf{k} = \partial_\phi, \tag{A.5}$$

since it is decomposed into the basis $\{\partial_\phi, \partial_\theta\}$ of the vector space attached to each point of the sphere. Obviously, other Killing vectors for the 2-sphere exist, and they correspond to rotations about the other axis x and y. However, it is less simple to guess them because the metric directly depends on the coordinate ϕ. A way to obtain these rotationnal Killing vectors is to express them in cartesian coordinates, and to convert them in polar coordinates. After these steps, one may get

$$\begin{aligned} \mathbf{r} &= \cos\phi\partial_\theta - \cot\theta\sin\phi\partial_\phi, \\ \mathbf{t} &= -\sin\phi\partial_\theta - \cot\theta\cos\phi\partial_\phi. \end{aligned} \tag{A.6}$$

Note that the mirror transformations $\phi \to -\phi$ and $\theta \to -\theta$ are not Killing vectors since they correspond to discrete, and not continuous, symmetries of the metric.

More formally, any vector $\mathbf{m}$ that satisfies the Killing's equation

$$\nabla_\mu m_\nu + \nabla_\nu m_\mu = 0 \tag{A.7}$$

is a Killing vector, and reciprocally. Any linear combination of Killing vectors is also a Killing vector. A corollary is that if the metric does not depend on a coordinate, then it admits at least a Killing vector. Therefore, we can systematically guess some Killing vectors without trying to solve the Killing's equation, as it was done for $\mathbf{k}$ in the 2-sphere.

One can also associate a constant of motion to a Killing vector $\mathbf{m}$. Indeed, it can be shown that the quantity

$$g_{\alpha\beta}u^{\alpha}m^{\beta} = u^{\alpha}m_{\alpha}, \tag{A.8}$$

is conserved along a geodesic, where u^{α} is the tangent vector to the geodesic of the particle and $g_{\alpha\beta}$ the metric tensor. For instance, consider a free massive particle immersed in the Minkowski spacetime

$$ds^2 = -dt^2 + dx^2 + dy^2 + dz^2. \tag{A.9}$$

The independance of the metric components with respect to t, x, y and z, yields four Killing vectors associated with time and space translations. Let us focus on the Killing vector $l_{\mu} = (0, 0, 0, 1)$ for the translation in the z-direction. The conserved quantity associated with l_{μ} is

$$u^{\alpha}l_{\alpha} = u^{z}, \tag{A.10}$$

which corresponds to the velocity of the free massive particle in the z direction. If we generalize this result to the other components of the four-velocity u^{α}, we get that the four-velocity of a free massive particle in the Minkoswki spacetime is conserved, as is expected.

B | Energy-momentum tensor

The symmetric stress-energy tensor of a minimally coupled, complex, spinless, massive scalar field is given by

$$T^{\mu}{}_{\nu} = \frac{1}{2}\left(\nabla^{\mu}\Phi^{*}\nabla_{\nu}\Phi + \nabla_{\nu}\Phi^{*}\nabla^{\mu}\Phi\right) - \delta^{\mu}{}_{\nu}\mathcal{L}, \tag{B.1}$$

where $\mathcal{L}$ is the free Lagrangian density of a scalar field Φ. Let us show that the energy-momentum tensor is conserved, which means that its covariant divergence cancels

$$\nabla_{\mu}T^{\mu\nu} = 0. \tag{B.2}$$

Indeed, by definition of the Lagrangian density (2.3), we get

$$\begin{aligned}
\nabla_{\mu}T^{\mu}{}_{\nu} &= \nabla_{\mu}\left(\frac{1}{2}\left(\nabla^{\mu}\Phi^{*}\nabla_{\nu}\Phi + \nabla_{\nu}\Phi^{*}\nabla^{\mu}\Phi\right) - \delta^{\mu}{}_{\nu}\mathcal{L}\right), \\
&= \frac{1}{2}\left[(\nabla_{\mu}\nabla^{\mu}\Phi^{*})\nabla_{\nu}\Phi + \nabla^{\mu}\Phi^{*}(\nabla_{\mu}\nabla_{\nu}\Phi) + (\nabla_{\mu}\nabla_{\nu}\Phi^{*})\nabla^{\mu}\Phi + \nabla_{\nu}\Phi^{*}(\nabla_{\mu}\nabla^{\mu}\Phi)\right. \\
&- \left.\frac{1}{2}\nabla_{\nu}(\partial^{\mu}\Phi^{*}\partial_{\mu}\Phi) - \frac{1}{2}\nabla_{\nu}(\partial_{\mu}\Phi^{*}\partial^{\mu}\Phi) + \mu^{2}\nabla_{\nu}|\Phi|^{2}\right].
\end{aligned}$$

Now, we can rearrange the terms and make use of the equation of motion (2.7) of a scalar field to simplify some terms:

$$\begin{aligned}
\nabla_{\mu}T^{\mu}{}_{\nu} &= \frac{1}{2}\left[(\nabla_{\mu}\nabla^{\mu}\Phi - \mu^{2}\Phi)\nabla_{\nu}\Phi^{*} + (\nabla_{\mu}\nabla^{\mu}\Phi^{*} - \mu^{2}\Phi^{*})\nabla_{\nu}\Phi + \nabla^{\mu}\Phi^{*}(\nabla_{\mu}\nabla_{\nu}\Phi)\right. \\
&+ \left.(\nabla_{\mu}\nabla_{\nu}\Phi^{*})\nabla^{\mu}\Phi - (\nabla_{\nu}\nabla_{\mu}\Phi^{*})\partial^{\mu}\Phi - (\nabla_{\nu}\nabla_{\mu}\Phi)\nabla^{\mu}\Phi^{*}\right] \\
&= \frac{1}{2}\nabla^{\mu}\Phi^{*}[\nabla_{\mu},\nabla_{\nu}]\Phi + \frac{1}{2}\nabla^{\mu}\Phi[\nabla_{\mu},\nabla_{\nu}]\Phi^{*},
\end{aligned}$$

where in the last line we used the definition of the commutator. Since the latter applies to a scalar quantity, it vanishes and we demonstrate the conservation law (B.2).

Bibliography

[1] E. P. Hubble. “Extragalactic nebulae.” In: *The Astrophysical Journal* 64 (1926), pp. 321–369.

[2] V. C. Rubin, Jr. Ford W. K., and N. Thonnard. “Extended rotation curves of high-luminosity spiral galaxies. IV. Systematic dynamical properties, Sa -> Sc.” In: *The Astrophysical Journal Letters* 225 (1978), pp. L107–L111.

[3] C. Alcock et al. “The MACHO Project: Microlensing results from 5.7 years of Large Magellanic Cloud observations”. In: *The Astrophysical Journal* 542.1 (2000), pp. 281–307.

[4] K. A. Olive, G. Steigman, and T. P. Walker. “Primordial nucleosynthesis: theory and observations”. In: *Physics Reports* 333-334 (2000), pp. 389–407.

[5] F. Zwicky. “Die Rotverschiebung von extragalaktischen Nebeln”. In: *Helvetica Physica Acta* 6 (1933), pp. 110–127.

[6] P. Natarajan E. Jullo and J-P. Kneib. *Abell 1689*. `https://hubblesite.org/resource-gallery/images`. Accessed: 28-7-2022.

[7] NASA and ESO collaboration. *Bullet cluster*. `https://supernova.eso.org/germany/exhibition/images/0811_B1/`. Accessed: 27-7-2022.

[8] M.J. Jee and A. Mahdavi. *Abell 520*. `https://www.nasa.gov/multimedia/imagegallery/image_feature_2189.html`.

[9] M. Markevitch D. Clowe et al. “On dark peaks and missing mass: a weak lensing mass reconstruction of the merging cluster system Abell 520”. In: *The Astrophysical Journal* 758.2 (2012), p. 128.

[10] F. Lanusse A. Peel and J. Starck. “Sparse reconstruction of the merging A520 cluster system”. In: *The Astrophysical Journal* 847.1 (2017), p. 23.

[11] Planck Collaboration et al. “Planck 2013 results. I. Overview of products and scientific results”. In: *Astronomy &amp Astrophysics* 571 (2014), A1.

[12] A. Friedmann. “Über die Krümmung des Raumes”. In: *Zeitschrift fur Physik* 10 (1922), pp. 377–386.

[13] A. Friedmann. “Über die Möglichkeit einer Welt mit konstanter negativer Krümmung des Raumes”. In: *Zeitschrift fur Physik* 21.1 (1924), pp. 326–332.

[14] G. Lemaıtre. “Un univers homogène de masse constante et de rayon croissant rendant compte de la vitesse radiale des nébuleuses extra-galactiques”. In: *Annales de la Société Scientifique de Bruxelles* (1927), pp. 49–59.

[15] G. Lemaıtre. “Expansion of the universe, a homogeneous universe of constant mass and increasing radius accounting for the radial velocity of extra-galactic nebulae”. In: *Monthly Notices of the Royal Astronomical Society* 91 (1931), pp. 483–490.

[16] H. P. Robertson. “Kinematics and World-structure”. In: *The Astrophysical Journal* 82 (1935), p. 284.

[17] H. P. Robertson. “Kinematics and World-structure II.” In: *The Astrophysical Journal* 83 (1936), p. 187.

[18] H. P. Robertson. “Kinematics and World-structure III.” In: *The Astrophysical Journal* 83 (1936), p. 257.

[19] A. G. Walker. “On Milne’s theory of World-structure”. In: *Proceedings of the London Mathematical Society* 42 (1937), pp. 90–127.

[20] S. D. Epps and M. J. Hudson. “The weak lensing masses of filaments between luminous red galaxies”. In: *Monthly Notices of the Royal Astronomical Society* 468.3 (2017), pp. 2605–2613.

[21] M. Boylan-Kolchin et al. “Resolving cosmic structure formation with the Millennium-II simulation”. In: *Monthly Notices of the Royal Astronomical Society* 398.3 (2009), pp. 1150–1164.

[22] E. G. M. Ferreira. “Ultra-light dark matter”. In: *The Astronomy and Astrophysics Review* 29.1 (2021).

[23] B. P. Abbott et al. “Observation of gravitational waves from a binary black Hole merger”. In: *Physical Review Letters* 116 (6 2016).

[24] A. Einstein. “Näherungsweise integration der feldgleichungen der gravitation”. In: *Sitzungsberichte der Königlich Preußischen Akademie der Wissenschaften (Berlin* (1916), pp. 688–696.

[25] R. A. Hulse and H. J. Taylor. “Discovery of a pulsar in a close binary system.” In: *Bulletin of the American Astronomical Society* 6 (1974), p. 453.

[26] J. H. Taylor and J. M. Weisberg. “A new test of general relativity - Gravitational radiation and the binary pulsar PSR 1913+16”. In: *The Astrophysical Journal* 253 (1982), pp. 908–920.

[27] M. Sieniawska and M. Bejger. “Continuous gravitational waves from neutron stars: current status and prospects”. In: *Universe* 5.11 (2019), p. 217.

[28] G Pagliaroli E. Abdikamalov and Da. Radice. “Gravitational waves from core-collapse supernovae”. In: *Handbook of Gravitational Wave Astronomy*. Springer Singapore, 2021, pp. 1–37.

[29] J. Weber. “Gravitational radiation”. In: *Physical Review Letters* 18.13 (1967), pp. 498–501.

[30] Virgo. *Aerial view of Virgo*. `https://news.cnrs.fr/articles/a-new-window-to-the-universe`. Accessed: 1-8-2022.

[31] MiniGRAIL. *Eugenio Coccia is exciting the quadrupole modes of the sphere*. `https://www.minigrail.nl/`. Accessed: 1-8-2022.

[32] S. Detweiler. “Klein-Gordon equation and rotating black holes”. In: *Physical Review D* 22.10 (1980), pp. 2323–2326.

[33] A. Arvanitaki and S. Dubovsky. "Exploring the string axiverse with precision black hole physics". In: *Phys. Rev. D* 83.4 (2011), p. 044026.

[34] D. Baumann, H. S. Chia, and R. A. Porto. "Probing ultralight bosons with binary black holes". In: *Physical Review D* 99.4 (2019).

[35] R. P. Kerr. "Gravitational field of a spinning mass as an example of algebraically special metrics". In: *Physycal Review Letters* 11 (5 1963), pp. 237–238.

[36] D. Baumann. *Gravitational collider physics - Seminar at Academia Sinica Institute of Astronomy and Astrophysics (ASIAA) in 2022.* `https://www.nasa.gov/multimedia/imagegallery/image_feature_2189.html`.

[37] A. Einstein. "Zur allgemeinen Relativitätstheorie". In: *Sitzungsberichte der Königlich Preußischen Akademie der Wissenschaften* (1915), pp. 778–786.

[38] K. Schwarzschild. "Über das gravitationsfeld eines massenpunktes nach der Einsteinschen theorie". In: *Sitzungsberichte der Königlich Preußischen Akademie der Wissenschaften (Berlin)* (1916), pp. 189–196.

[39] J. R. Oppenheimer and H. Snyder. "On continued gravitational contraction". In: *Physical Review* 56.5 (1939), pp. 455–459.

[40] E. T. Newman et al. "Metric of a rotating, charged mass". In: *Journal of Mathematical Physics* 6.6 (1965), pp. 918–919.

[41] P. K. Townsend. "Black holes". In: *arXiv e-prints* (1997).

[42] M. Zajaček and A. Tursunov. "Electric charge of black holes: Is it really always negligible?" In: *arXiv* (2019).

[43] G. C. Debney, R. P. Kerr, and A. Schild. "Solutions of the Einstein and Einstein-Maxwell Eeuations". In: *Journal of Mathematical Physics* 10.10 (1969), pp. 1842–1854.

[44] S. R. Dolan and D. Dempsey. "Bound states of the Dirac equation on Kerr spacetime". In: *Classical and Quantum Gravity* 32.18 (2015), p. 184001.

[45] M. Visser. "The Kerr spacetime: A brief introduction". In: *arXiv e-prints* (2007).

[46] R. M. Wald. *General Relativity.* University of Chicago Press, 1984.

[47] R. Penrose and R. M. Floyd. "Extraction of rotational energy from a black hole". In: *Nature Physical Science* 229.6 (1971), pp. 177–179.

[48] S. M. Carroll. *Spacetime and geometry. An introduction to General relativity.* Cambridge University Press, 2004.

[49] D. R. Brill et al. "Solution of the scalar wave equation in a Kerr background by separation of variables". In: *Physical Review D* 5.8 (1972), pp. 1913–1915.

[50] S. R. Dolan. "Instability of the massive Klein-Gordon field on the Kerr spacetime". In: *Physical Review D* 76.8 (2007).

[51] E. Poisson. *A relativist's toolkit : the mathematics of black-hole mechanics.* Cambridge University Press, 2004.

[52] H. Furuhashi and Y. Nambu. "Instability of massive scalar fields in Kerr-Newman spacetime". In: *Progress of Theoretical Physics* 112.6 (2004), pp. 983–995.

[53] W. H. Press et al. *Numerical recipes in C. The art of scientific computing*. Cambridge University Press, 1992.

[54] Y. Huang and D. Liu. "Scalar clouds and the superradiant instability regime of Kerr-Newman black hole". In: *Physical Review D* 94.6 (2016).

[55] S. R. Dolan. "Superradiant instabilities of rotating black holes in the time domain". In: *Physical Review D* 87.12 (2013).

[56] R. Brito, V. Cardoso, and P. Pani. *Superradiance*. Springer International Publishing, 2020.

[57] D. Baumann et al. "Ionization of gravitational atoms". In: *Physical Review D* 105.11 (2022).

[58] M. Maggiore. *Gravitational waves: Volume 1: Theory and experiments*. Oxford University Press, 2007.

[59] S. Weinberg. *Gravitation and cosmology: Principles and applications of the General theory of Relativity*. Wiley (New-York), 1972.

[60] A. Arvanitaki, M. Baryakhtar, and X. Huang. "Discovering the QCD axion with black holes and gravitational waves". In: *Physical Review D* 91.8 (2015), p. 084011.